Two-dimensional random-bond Ising model, free fermions, and the network model

F. Merz and J. T. Chalker

Theoretical Physics, University of Oxford, 1 Keble Road, Oxford OX1 3NP, United Kingdom

We develop a recently proposed mapping of the two-dimensional Ising model with random exchange (RBIM) via the transfer matrix, to a network model for a disordered system of noninteracting fermions. The RBIM transforms in this way to a localization problem belonging to one of a set of nonstandard symmetry classes, known as class D; the transition between paramagnet and ferromagnet is equivalent to a delocalization transition between an insulator and a quantum Hall conductor. We establish the mapping as an exact and efficient tool for numerical analysis: using it, the computational effort required to study a system of width M is proportional to M^3, and not exponential in M as with conventional algorithms. We show how the approach may be used to calculate for the RBIM the free energy, typical correlation lengths in quasi-one dimension for both the spin and the disorder operators, and the even powers of spin-spin correlation functions and their disorder averages. We examine in detail the square-lattice, nearest-neighbor $\pm J$ RBIM, in which bonds are independently antiferromagnetic with probability p, and ferromagnetic with probability $1-p$. Studying temperatures $T \geq 0.4J$, we obtain precise coordinates in the $p-T$ plane for points on the phase boundary between ferromagnet and paramagnet, and for the multicritical (Nishimori) point. We demonstrate scaling flow towards the pure Ising fixed point at small p, and determine critical exponents at the multicritical point.

I. INTRODUCTION

The two-dimensional Ising model[1,2] has been a basic prototype in the theory of phase transitions for over half a century. A central factor in its importance has been its equivalence to a system of noninteracting fermions, as set out by Schultz, Mattis, and Lieb[3] in their well-known reformulation of Onsager's solution. The two-dimensional Ising model has naturally also been a test bed for studies of the effect of quenched disorder on phase transitions, and the equivalence between the spin system and free fermions continues to hold in the presence of randomness in exchange interactions. In this paper we build on recent work by Cho and Fisher[4,5] and by Gruzberg, Read, and Ludwig[6,7] to establish the correspondence in a form suitable for numerical analysis, and use it to study the square-lattice, random-bond Ising model (RBIM).

The consequences for the two-dimensional Ising model of weak randomness in exchange interactions are rather well understood, following analytical calculations based on the Fermionic formulation by Dotsenko and Dotsenko[8] and others:[9–11] weak disorder is marginally irrelevant in the renormalization group sense, and the thermally driven transition from the paramagnet to the ferromagnet survives with only logarithmic modifications to the critical behavior of the pure system. By contrast, strong disorder has more dramatic effects. A convenient choice is to consider exchange interactions with fixed magnitude which are independently ferromagnetic or antiferromagnetic, with probabilities $1-p$ and p, respectively. In this case, it is known from a variety of approaches[12–29] that the Curie temperature is depressed with increasing p, reaching zero at a critical disorder strength p_c. Moreover, while the scaling flow at the transition is controlled for small p by the critical fixed point of the pure system, at larger p it is determined by a disorder-dominated multicritical point, known as the Nishimori point.[14–16]

Most numerical studies of the RBIM have used either

Monte Carlo simulations[19,20] or transfer-matrix calculations in a spin basis.[21–27] Fermionic formulations of the Ising model nevertheless have two great potential advantages: they can avoid the statistical sampling errors of Monte Carlo simulations; and also, if implemented using the transfer matrix, they can avoid the exponential growth in transfer-matrix dimension with system width that occurs if this matrix is written in a spin basis. Pioneering steps in the first of these directions have been taken by Blackman[30] and collaborators,[31] and others,[32–34] using the solution of the two-dimensional Ising model via a Pfaffian[2] to express statistical-mechanical quantities in terms of spectral properties of the associated matrix. Their work makes a link between the RBIM and localization problems, since the matrix allied to the Pfaffian is essentially a tight-binding Hamiltonian on the lattice of the underlying Ising model, with random hopping arising from random exchange. An alternative route from the RBIM to a localization problem has been proposed by Cho and Fisher:[4,5] starting from two copies of the transfer matrix for an Ising model, each expressed in terms of Majorana fermions and combined to form Dirac fermions, they arrive at a version of the network model similar to that introduced as a description for the integer quantum Hall plateau transition,[35] though with a distinct symmetry.

Viewed as a localization problem, the paramagnetic and ferromagnetic phases of the RBIM translate to two insulating phases with Hall conductance differing by one quantum unit, while the Curie transition maps to a version of the quantum Hall plateau transition. This transition, and indeed the insulating phases, belong to a nonstandard symmetry class for localization, classified in work by Altland and Zirnbauer[36] and known as class D. The match between behavior expected in the RBIM and that anticipated for two-dimensional localization problems in class D has been the subject of recent discussion.[6,7,37–41] A particular difficulty has been to reconcile the fact that, generically, a third, metallic phase is pos-

sible in the localization problem, in addition to the two insulating phases, while the RBIM in two dimensions is expected to display only two phases. The resolution which has emerged[6,41] is that symmetry alone is not sufficient to determine the phases that appear, and that in the specific disordered conductor equivalent to the RBIM no metallic phase arises.

The work we describe here builds on Cho and Fisher's ideas, which must be extended in several ways to provide a precise and practical treatment of the RBIM. First, the approach described in Ref. 4 proceeds from the RBIM via a continuum limit, which is rediscretized to obtain a network model. In order to find an explicit relationship between parameters in the two systems, it is necessary instead to carry out the mapping directly on a lattice model. Doing so, as described by Cho in her thesis[5] and by Gruzberg, Read, and Ludwig in Refs. 6 and 7, one arrives at a network model different in detail to that studied in Ref. 4, and with different behavior.[41] Second, a proper treatment of the RBIM in cylindrical geometry requires an appropriate choice of boundary conditions in the network model, which has not previously been considered. Third, to calculate thermodynamic quantities, typical correlation lengths, spin, and disorder correlation functions for the RBIM using the network model formulation, it is necessary to map from fermions back to spins, as outlined in Refs. 6 and 7 and as we describe here. A feature of interest which emerges from our analysis is a topological distinction between the paramagnetic and ferromagnetic phases as represented in terms of fermions, similar to that discussed recently for other systems from symmetry class D.[6,42] Finally, an important technical aspect of the work we present here is that numerical transfer-matrix calculations for localization problems in the symmetry class we are concerned with require for numerical stability a modification of the standard algorithm, as discussed in Ref. 41.

As a numerical approach to the RBIM, the method we describe has two main limitations. One arises because the Dirac fermions of the network model are built from two copies of an Ising model. As a result, it turns out to be straightforward to calculate even powers of spin-correlation functions, and their disorder averages, but not practical to calculate odd powers. The other stems from the fact that Boltzmann factors which enter the network model become large at low temperatures, making the zero-temperature limit inaccessible.

The remainder of the paper is organized as follows: In Secs. II A and II B we outline the Jordan-Wigner Fermionization of the spin transfer matrix and the mapping to a network model. In Sec. II C we discuss boundary conditions across the system in network model language and the subsequent rules for constructing the spin transfer matrix from the fermion transfer matrix. In Sec. III and the Appendix we review the numerical algorithm that we employ in the network model transfer-matrix calculations and set out how statistical-mechanical quantities are obtained from the fermion description. In Sec. IV we present numerical results on the $\pm J$ RBIM. The system sizes we study (transverse width $M=8-256$ spins) are significantly larger than what was previously possible. We focus on critical behavior at the Nishi-
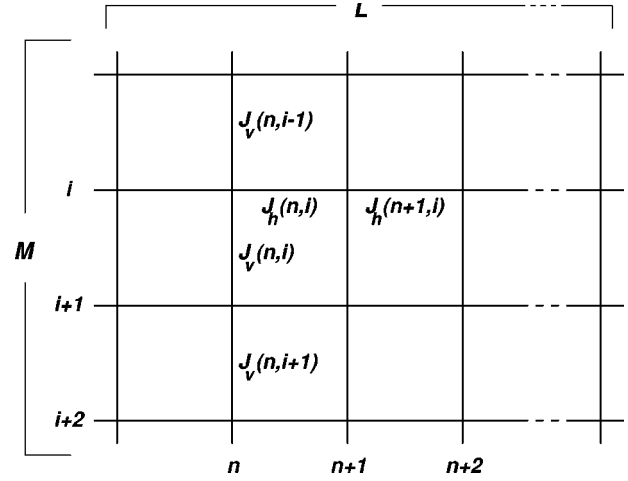

FIG. 1. For the square lattice Ising model we adopt the convention that a pair (n,i) labels one spin with two associated bonds, one horizontal (to the right) and one vertical (downwards).

mori point, for which we determine the coordinate $p_c = 0.1093 \pm 0.0002$. We calculate the critical exponents ν and ν_T, describing the divergence of the correlation length as the Nishimori point is approached along the Nishimori line and the phase boundary, respectively. Using large system sizes we find $\nu = 1.50 \pm 0.03$, in disagreement with previous estimates,[18,27] and, with wider confidence limits, $\nu_T = 4.0 \pm 0.5$.

II. TRANSFER MATRIX

A. Ising model transfer matrix

We consider the nearest-neighbor Ising model on a square lattice in two dimensions. The partition function Z for a such a system on a strip of length L and width M can be written[1] in terms of a product of transfer matrices. Introducing integer coordinates n and i, as illustrated in Fig. 1, one has

$$Z = \mathcal{A}\mathrm{Tr}[\hat{T}_1 \hat{T}_2 \cdots \hat{T}_n \cdots \hat{T}_L], \tag{1}$$

with $\hat{T}_n = \hat{V}_n \times \hat{H}_n$ and

$$\hat{H}_n = \exp\left(-\sum_{i=1}^{M} [\kappa^*_{n,i} \sigma^z_i] \right),$$

$$\hat{V}_n = \exp\left(\sum_{i=1}^{M} [\kappa_{n,i} \sigma^x_i \sigma^x_{i+1}] \right), \tag{2}$$

where the σ's are Pauli matrices and

$$\kappa_{n,i} = \beta J_v(n,i),$$

$$\kappa^*_{n,i} = -\frac{1}{2}\ln[\tanh \beta J_h(n,i)],$$

$$\mathcal{A} = \prod_{n=1}^{L} \prod_{i=1}^{M} \sqrt{2}[\sinh 2\kappa^*_{n,i}]^{-1/2}. \tag{3}$$

Here, $\kappa_{n,i}$ is the reduced coupling strength at inverse temperature β between the ith and $(i+1)$th spin in the vertical direction of Fig. 1 on the nth slice, and $\kappa_{n,i}^*$ is the Kramers-Wannier dual value of the corresponding bond strength in the horizontal direction. For the rest of the paper the labels v and h on the bond strengths are redundant, since all horizontal bond strengths (and only those) appear as dual values, identified with an asterisk. We take $\sigma_{M+1}^x \equiv \sigma_1^x$ in Eq. (2) so that boundary conditions across the strip are controlled by the set of interactions strengths $\kappa_{n,M}$. For convenience we introduce the notation $\hat{T}(k,l) \equiv \Pi_{n=k}^{l} \hat{T}_n$, and for brevity we use $\hat{T}$ to denote either $\hat{T}(k,l)$ or $\hat{T}_n$.

Following Schultz, Mattis, and Lieb[3] the operators $\hat{H}_n$ and $\hat{V}_n$ can be written, using the Jordan-Wigner-transformation, as functions of Fermionic operators. Introducing the fermion annihilation and creation operators C_i and $C_i^\dagger$, the spin operators become

$$\sigma_i^x = \exp\left(i\pi \sum_{j=1}^{i-1} C_j^\dagger C_j \right)(C_i^\dagger + C_i),$$

$$\sigma_i^z = 2C_i^\dagger C_i - 1. \qquad (4)$$

After Jordan-Wigner transformation, $\hat{H}_n$ and $\hat{V}_n$ read

$$\hat{H}_n = \exp\left(-2\sum_{i=1}^{M} \kappa_{n,i}^* \left[C_i^\dagger C_i - \frac{1}{2} \right] \right),$$

$$\hat{V}_n = \exp\left(\sum_{i=1}^{M-1} \kappa_{n,i} [C_i^\dagger - C_i][C_{i+1}^\dagger + C_{i+1}] \right.$$

$$\left. - \kappa_{n,M} e^{i\pi N_C} [C_M^\dagger - C_M][C_1^\dagger + C_1] \right), \qquad (5)$$

with $N_C = \Sigma_{i=1}^{M} C_i^\dagger C_i$, the number operator. A familiar feature of the transfer matrix in Fermionic language is that it does not conserve N_C, since $\hat{V}_n$ includes terms which create and annihilate fermions in pairs. Such a structure is reminiscent of Bogoliubov–de Gennes Hamiltonians arising in the mean-field description of superconductors. It has the consequence that, to diagonalize the transfer matrix for a translationally invariant Ising model, one uses Fourier transformation followed by Bogoliubov transformation. For the RBIM without translational invariance, the transformation that diagonalizes the transfer matrix is disorder dependent, and one must follow a different route to make progress.

In place of diagonalization, the objective for the RBIM is to write the transfer matrix in terms of Dirac fermions whose number is conserved under its action. The necessary steps are well-established[43,10] and have been set out in the present context by Cho and Fisher,[4] Cho,[5] and Gruzberg, Read, and Ludwig.[7] First, because of the form of Eq. (5), it is natural to decompose the complex (Dirac) fermions into real and imaginary parts, introducing real (Majorana) fermions ξ_C and η_C. Suppressing the site index one can write

$$C = \frac{1}{\sqrt{2}}[\xi_C - i\eta_C], \quad C^\dagger = \frac{1}{\sqrt{2}}[\xi_C + i\eta_C], \qquad (6)$$

where ξ_C and η_C anticommute and satisfy $\xi_C^\dagger = \xi_C$, $\eta_C^\dagger = \eta_C$ and $\{\xi_{Ci}, \xi_{Cj}\} = \{\eta_{Ci}, \eta_{Cj}\} = \delta_{ij}$. Next, in order to return to Dirac fermions, one introduces a second, identical copy of the Ising model. We represent the second copy using the Dirac fermions D and $D^\dagger$, in analogy to the C and $C^\dagger$, and employ the Majorana decomposition $D = [\xi_D - i\eta_D]/\sqrt{2}$ and $D^\dagger = [\xi_D + i\eta_D]/\sqrt{2}$. This provides different ways to recombine the Majorana fermions. Of the various alternatives, consider in particular the Dirac fermions $f = [\xi_C + i\xi_D]/\sqrt{2}$ and $g = [\eta_D - i\eta_C]/\sqrt{2}$, which we choose to yield real coefficients later on. Again suppressing the site index, this transformation may be summarized by

$$C = \frac{1}{2}[f + f^\dagger + g - g^\dagger],$$

$$D = \frac{i}{2}[f^\dagger - f - g - g^\dagger], \qquad (7)$$

and its inverse

$$f = \frac{1}{2}[C + C^\dagger + iD + iD^\dagger],$$

$$g = \frac{1}{2}[C - C^\dagger + iD - iD^\dagger]. \qquad (8)$$

As an aside, we note that the Jordan-Wigner transformation applied to two copies of the Ising model does not by itself generate the correct commutation relations between pairs of spin operators σ^x taken one from each copy. To ensure these commutation relations one should in addition introduce Klein factors. Since the Klein factors ultimately have no effect on the equations we present, we omit them throughout this paper.

For the doubled system, we are concerned with the transfer-matrix products (suppressing the slice index) $\hat{H}_C \hat{H}_D$ and $\hat{V}_C \hat{V}_D$. The value of the transformation Eq. (7) is that it reduces these products to the simple forms

$$\hat{H}_C \hat{H}_D = \exp\left(-2\sum_{i=1}^{M} \kappa_{n,i}^* [g_i^\dagger f_i + f_i^\dagger g_i] \right),$$

$$\hat{V}_C \hat{V}_D = \exp\left(2\sum_{i=1}^{M-1} \kappa_{n,i} [g_i^\dagger f_{i+1} + f_{i+1}^\dagger g_i] + B \right), \qquad (9)$$

where the boundary term B is

$$B = -\kappa_{n,M}[(e^{i\pi N_C} + e^{i\pi N_D})[g_M^\dagger f_1 + f_1^\dagger g_M]$$

$$+ (e^{i\pi N_C} - e^{i\pi N_D})[g_M^\dagger f_1^\dagger + f_1 g_M]]. \qquad (10)$$

This process of doubling the degrees of freedom and rewriting them locally as fermions, in order to remove terms which are not particle conserving, may be viewed as a local Bogoliubov transformation.

The boundary term B contains the two boundary operators

$$\mathcal{B}^{\pm} = e^{i\pi N_C} \pm e^{i\pi N_D}. \tag{11}$$

These operators commute with the transfer matrix as a consequence of Z_2 symmetry: for a single system, say C, one can identify two invariant subspaces, distinguished by the behavior of vectors within the subspace under the operation $\hat{R}_C$ which reverses the orientation of a complete row of spins.[1] Specifically,

$$\hat{R}_C = \prod_i \sigma_{iC}^z,$$

$$\hat{R}_C \sigma_{jC}^x \hat{R}_C = -\sigma_{jC}^x \tag{12}$$

for all j, and $\hat{R}_C^2 = 1$. Introducing the corresponding operator $\hat{R}_D$ for the D system and assuming the total number of spins across the strip to be even, one finds that the boundary operators are simply $\mathcal{B}^{\pm} = \hat{R}_C \pm \hat{R}_D$. Since both $\hat{R}_C$ and $\hat{R}_D$ commute with the transfer matrix, four invariant subspaces arise naturally from $[\hat{R}_C = \pm 1] \otimes [\hat{R}_D = \pm 1]$. Using obvious notation, $\hat{T}_C \hat{T}_D$ may then be presented schematically in the block-diagonal form

$$\hat{T}_C \hat{T}_D = \begin{pmatrix} ++ & 0 & 0 & 0 \\ 0 & -+ & 0 & 0 \\ 0 & 0 & +- & 0 \\ 0 & 0 & 0 & -- \end{pmatrix}. \tag{13}$$

Thus the Fock space associated with the C and D fermions can be divided into four subspaces according to the parity of N_C and N_D. In two of them, for which $\mathcal{B}^- = 0$, the number of f and g fermions is conserved under the action of $\hat{T}$.

B. Network model interpretation

The conservation of the Dirac fermions f and g under the action of the transfer-matrix operator makes it possible to go from a second-quantized description to a first-quantized form. Moreover, just as the second-quantized form has SO(2) symmetry,[7] one finds that the first-quantized form may be interpreted as the transfer matrix for a scattering problem, because it fulfills the requirements arising from unitarity of the scattering matrix. Specifically, the first-quantized form represents a network model, in which noninteracting f and g fermions propagate on directed links of a lattice. The fermions scatter at nodes, where two incoming links and two outgoing links meet. In this way, the nodes of the network model take the place of bonds in the Ising model. A correspondence of this type was set out by Cho and Fisher[4] and subsequently refined by Cho,[5] who pointed out that the network model studied numerically in Ref. 4 is equivalent to an Ising model in which some exchange couplings are imaginary, while the RBIM itself is represented by a different network model. In this subsection we review these ideas.

The identification of the first-quantized form of $\hat{T}$ makes use of a general equivalence between first- and second-
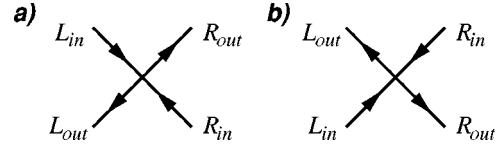

FIG. 2. Scattering nodes for: (a) horizontal and (b) vertical bonds.

quantized versions of linear transformations. Consider in a Hilbert space of dimension N a linear transformation of single-particle wave functions, represented in a certain basis by an $N \times N$ matrix with elements $(\exp G)_{ij}$. Introducing in the same basis fermion creation and annihilation operators, $\alpha_i^{\dagger}$ and α_i, the second-quantized representation of this transformation is $\exp[\alpha_i^{\dagger} G_{ij} \alpha_j]$. To apply this equivalence to the transfer matrix $\hat{T}$, let the $N \equiv 2M$ fermion annihilation operators be $[\alpha_1, \ldots, \alpha_{2M}] = [f_1, \ldots, f_M, g_1, \ldots, g_M]$. In the $\mathcal{B}^- = 0$ subspaces, the transfer matrix of the RBIM has the canonical form

$$\hat{T}_C \hat{T}_D = \exp[\alpha_i^{\dagger} G_{ij} \alpha_j], \tag{14}$$

and can be represented equivalently by the $2M \times 2M$ matrix T, with elements $T_{ij} = (\exp G)_{ij}$, as a transformation of single-particle states. Thus the action of the operator $\hat{T}$ on a Slater determinant is replicated by the action of the matrix T on the orbitals entering the determinant. In the following we use notation for the matrix T corresponding to that introduced for the operator $\hat{T}$: T_n denotes the transfer matrix for the nth slice of the system, $T(k,l)$ indicates a product, and T is shorthand for either.

While knowledge of the single-particle form of T is enough by itself for efficient numerical calculations, physical interpretation within this framework of the RBIM as a localization problem depends on the fact that T is a pseudo-orthogonal matrix. In consequence, it can be viewed as the transfer matrix for a scattering problem in which flux is conserved. In order to see that this is indeed the case, consider the basic building blocks of the transfer matrix for one column of sites in the doubled Ising model. The two factors, $\hat{H}_D \hat{H}_C$ and $\hat{V}_D \hat{V}_C$, appearing in Eq. (2) each consist of products of M commuting operators. Every such operator represents a single bond of the Ising model and involves only one pair of f and g fermions. Schematically, a horizontal bond gives rise to $\exp(-2\kappa^*[g^{\dagger}f + f^{\dagger}g])$, which is replaced in a first-quantized treatment by the 2×2 matrix $h \equiv \exp(-2\kappa^* \sigma^x)$, while a vertical bond yields $\exp(2\kappa[g^{\dagger}f + f^{\dagger}g])$, which is replaced by $v \equiv \exp(2\kappa \sigma^x)$. To arrive at a scattering problem, the f fermions are regarded (arbitrarily) as right movers, and the g fermions as left movers. Then the matrices h and v are transfer matrices for nodes of the network model. They relate flux amplitudes, L_{in} and L_{out}, to the amplitudes R_{in} and R_{out}, appearing either side of a node as illustrated in Fig. 2.

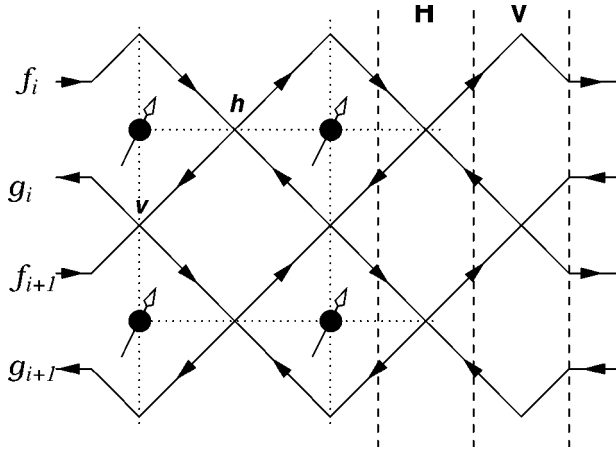In algebraic terms, we have for horizontal bonds the equation

FIG. 3. The network model. Flux propagates on links in the direction indicated by arrows. The transfer matrix relates flux amplitudes carried by links on the right to those on the left. Nodes arising from single rows of vertical bonds and horizontal bonds in the Ising model are indicated by V and H, respectively. Two particular nodes are labeled by h and v. Four sites of the Ising model are also shown with exchange interactions as dotted lines.

$$\begin{pmatrix} R_{out} \\ R_{in} \end{pmatrix} = \begin{pmatrix} \cosh 2\kappa^* & -\sinh 2\kappa^* \\ -\sinh 2\kappa^* & \cosh 2\kappa^* \end{pmatrix} \begin{pmatrix} L_{in} \\ L_{out} \end{pmatrix} \quad (15)$$

and for vertical bonds the equation

$$\begin{pmatrix} R_{in} \\ R_{out} \end{pmatrix} = \begin{pmatrix} \cosh 2\kappa & \sinh 2\kappa \\ \sinh 2\kappa & \cosh 2\kappa \end{pmatrix} \begin{pmatrix} L_{out} \\ L_{in} \end{pmatrix}. \quad (16)$$

Flux conservation follows from the relations $\sigma^z h^\dagger \sigma^z = h^{-1}$ and $\sigma^z v^\dagger \sigma^z = v^{-1}$.

The network model as a whole is illustrated in Fig. 3. It has the same structure as the U(1) network model, introduced to describe localization in the context of the integer quantum Hall effect.[35] Directed links form plaquettes, each with a definite sense of circulation, which is alternately clockwise and anticlockwise on successive squares. Disorder appears in the U(1) network model in the form of quenched random phases associated with links. By contrast, for the RBIM randomness enters only through the scattering parameters, 2κ and $2\kappa^*$, associated with nodes. An antiferromagnetic vertical bond leads to a negative node parameter, κ. An antiferromagnetic horizontal bond, however, gives rise to a complex κ^*, since from Eq. (3)

$$(-|\kappa|)^* = |\kappa|^* + i\pi/2, \quad (17)$$

generating an overall minus sign for h. The sign is accompanied by a minus sign as a factor in the coefficient $\mathcal{A}^2$, defined in Eq. (3).

The form of this disorder determines the symmetry class to which this network model belongs in the classification introduced by Altland and Zirnbauer.[36] Specifically, Hamiltonians H belonging to class D have, in a suitable basis, the property that $H^* = -H$, so that H is pure imaginary. Adapting this defining relation to a network model, one supposes that propagation on the network is generated by a time-evolution operator for unit time step, $\exp(iH)$. For class D,

this evolution operator is real, so that scattering phase factors may take only the values ± 1, as is indeed the case for the RBIM. In detail, a single antiferromagnetic bond (either horizontal or vertical) introduces phases of π for propagation around both the anticlockwise plaquettes that meet at the corresponding node, compared to the phases in the purely ferromagnetic model. Other choices of randomness belonging to the same symmetry class are of course possible. Cho and Fisher[4] investigated a model in which the transfer matrices at all nodes are of the type given in Eq. (16), with randomness in the sign of κ, while other authors[6,41] have studied a model in which scattering phase factors of ± 1 are associated independently with links rather than nodes. Strikingly, each of these different choices leads to very different localization properties in the network model.[6,41]

Combining the 2×2 transfer matrices, h or v, for each node, one arrives at the $2M \times 2M$ transfer matrix T for the system as a whole. Flux conservation guarantees that T may be factorized as

$$T = \begin{pmatrix} W_L & 0 \\ 0 & V_L^T \end{pmatrix} \begin{pmatrix} \cosh(\epsilon L) & \sinh(\epsilon L) \\ \sinh(\epsilon L) & \cosh(\epsilon L) \end{pmatrix} \begin{pmatrix} W_R^T & 0 \\ 0 & V_R \end{pmatrix}, \quad (18)$$

where components in the basis are ordered so that the amplitudes for propagation in one direction constitute the first M entries of the vectors on which T acts, and those for propagation in the opposite direction make up the remaining M entries. Here, the $M \times M$ matrices, W_L, W_R, V_L, and V_R are for a general localization problem unitary matrices, and for the Ising model orthogonal matrices, since in that case every element of the transfer matrix is real. The $M \times M$ matrix ϵ is real, positive and diagonal. It is convenient to rewrite Eq. (18) in the form

$$T = \frac{1}{2} \begin{pmatrix} W_L & -W_L \\ V_L^T & V_L^T \end{pmatrix} \begin{pmatrix} e^{\epsilon L} & 0 \\ 0 & e^{-\epsilon L} \end{pmatrix} \begin{pmatrix} W_R^T & V_R \\ -W_R^T & V_R \end{pmatrix}, \quad (19)$$

where the diagonal elements of $\exp(\pm \epsilon L)$ are the singular values of T. For a random system of length L, the exponents ϵL are $\mathcal{O}(L)$, with sample-to-sample fluctuations which are $\mathcal{O}(L^{1/2})$. From Oseledec's theorem, the average ϵ tends to a limit, $\mathrm{diag}(\epsilon_1, \epsilon_2, \ldots, \epsilon_M)$, for large L, where $\epsilon_1 \leq \epsilon_2 \leq \cdots \epsilon_M$ are the Lyapunov exponents characterizing the network model.

It is useful also to express Eq. (19) in second-quantized notation. Writing the left and right orthogonal matrices in terms of the Hermitian $2M \times 2M$ matrices A_L and A_R, defined by

$$\exp[-iA_L] \equiv \frac{1}{\sqrt{2}} \begin{pmatrix} W_L & -W_L \\ V_L^T & V_L^T \end{pmatrix},$$

$$\exp[iA_R] \equiv \frac{1}{\sqrt{2}} \begin{pmatrix} W_R^T & V_R \\ -W_R^T & V_R \end{pmatrix}, \quad (20)$$

the transfer matrix for the doubled Ising model takes the form (within the subspaces with $\mathcal{B}^- = 0$)

$$\hat{T}_C\hat{T}_D = \exp[-i\alpha_i^\dagger A_{Lij}\alpha_j] \times \exp[\alpha_i^\dagger\alpha_i[\sigma^z\otimes\epsilon L]_{ii}]$$
$$\times \exp[i\alpha_i^\dagger A_{Rij}\alpha_j]. \tag{21}$$

C. Lyapunov exponent spectrum

In this subsection we discuss some aspects of the mapping between the RBIM and the network model, which we have not considered before. These stem from the fact that, under the Jordan-Wigner transformation, different boundary conditions arise in $\hat{T}$ according to the parity of the fermion numbers N_C and N_D [see Eq. (10)]. Full information on sectors of both parities is contained in the results of network model calculations for the subspaces denoted $++$ and $--$ in Eq. (13). To make use of this information it is necessary establish how the Lyapunov exponents of the spin transfer matrix are related to those of the network model. A crucial step is to be able to identify the parity of left and right vectors of $\hat{T}$ when these are written in terms of the f and g fermions. We show here how this may be done.

As a starting point, consider the polar decomposition of the transfer matrix for the doubled Ising model, which takes the form

$$\hat{T}_C\hat{T}_D = \sum_{i,j=1}^{2^M} |L_{iC}\rangle\otimes|L_{jD}\rangle e^{(\lambda_i+\lambda_j)L}\langle R_{jD}|\otimes\langle R_{iC}|. \tag{22}$$

Here, $\{|L_{iC}\rangle\otimes|L_{jD}\rangle\}$ and $\{\langle R_{jD}|\otimes\langle R_{iC}|\}$ are two complete, orthonormal sets of many-particles states for the C and D fermions, which in general are not bi-orthogonal. The factors $e^{\lambda_i L}$ are the singular values of the transfer matrix for a single copy of the spin system, and the limiting values of λ_i for large L are the Lyapunov exponents characterizing the spin system. For economy, we use the same symbol to denote both the disorder-dependent λ_i at finite L and its limiting value as $L\rightarrow\infty$. Since we are concerned with the largest few singular values, we adopt the ordering $\lambda_1\geqslant\lambda_2\geqslant\cdots\geqslant\lambda_{2M}$.

Comparing Eq. (21) with Eq. (22), one sees that the values taken by $\exp(\alpha_i^\dagger\alpha_i[\sigma^z\otimes\epsilon L]_{ii})$ for $\alpha_i^\dagger\alpha_i=0$ or 1 generate the possible values of $e^{(\lambda_i+\lambda_j)L}$. In particular, ignoring for the moment questions connected with parity, the largest of the Lyapunov exponents for the doubled Ising model is obtained by setting $\alpha_i^\dagger\alpha_i=1$ for $1\leqslant i\leqslant M$ and $\alpha_i^\dagger\alpha_i=0$ for $M+1\leqslant i\leqslant 2M$. The associated right vector is

$$|\Psi\rangle\equiv|R_{1C}\rangle\otimes|R_{1D}\rangle=\prod_{i=1}^{M}\frac{1}{\sqrt{2}}[W_{ij}^Tf_j^\dagger+V_{ij}g_j^\dagger]|\text{vac}\rangle, \tag{23}$$

where $|\text{vac}\rangle$ is the vacuum for f and g fermions, and for simplicity we have omitted the subscript R on W and V. The state $|\Psi\rangle$ satisfies for all i the equations

$$[W_{ij}^Tf_j^\dagger+V_{ij}g_j^\dagger]|\Psi\rangle=0 \tag{24}$$

and

$$[W_{ij}^Tf_j-V_{ij}g_j]|\Psi\rangle=0. \tag{25}$$

Let $P=\frac{1}{2}[W^T-V]$ and $Q=\frac{1}{2}[W^T+V]$. Taking the difference between Eq. (24) and Eq. (25) yields $\gamma_i^\dagger|\Psi\rangle=0$ for all i, where the fermion creation operators $\gamma_i^\dagger$ are defined by

$$\gamma_i^\dagger=P_{ij}C_j+Q_{ij}C_j^\dagger. \tag{26}$$

[Of course, similar expressions for the D system may be obtained from the sum of Eq. (24) and Eq. (25).] In this way we find that the right vector associated with the largest possible singular value of the spin transfer matrix is

$$|R_{1C}\rangle=\prod_{i=1}^{M}\gamma_i^\dagger|0\rangle, \tag{27}$$

where $|0\rangle$ is the vacuum for the γ fermions. More generally, we can obtain all the right vectors as follows. First, in the factor $\exp(\alpha_i^\dagger\alpha_i[\sigma^z\otimes\epsilon L]_{ii})$ from Eq. (21), for each i in the range $1\leqslant i\leqslant M$ either: (i) set $\alpha_i^\dagger\alpha_i=1$ and $\alpha_{i+M}^\dagger\alpha_{i+M}=0$; or (ii) set $\alpha_i^\dagger\alpha_i=0$ and $\alpha_{i+M}^\dagger\alpha_{i+M}=1$. The corresponding right vector $|R\rangle$ satisfies for (i) $\gamma_i^\dagger|R\rangle=0$ and for (ii) $\gamma_i|R\rangle=0$. The associated Lyapunov exponents for the (undoubled) Ising model are

$$\lambda_j=\sum_{i=1}^{M}\epsilon_i\left(\gamma_i^\dagger\gamma_i-\frac{1}{2}\right), \tag{28}$$

where $\gamma_i^\dagger\gamma_i=1$ or 0 for (i) and (ii), respectively.

As a further step in the discussion, it is necessary to distinguish between the two sectors with even and odd parity for the fermion numbers N_C and N_D. Except in strip geometry [$\kappa_{n,M}=0$ in Eq. (10)], different boundary conditions are imposed on the network model for each sector, and so each sector has its own set of Lyapunov exponents ϵ and matrices W and V. We indicate quantities calculated using boundary conditions appropriate for even and odd parity sectors with plus and minus signs, respectively: $\epsilon^\pm$, $W^\pm$, and $V^\pm$. Introducing the number operator for γ fermions, $N_\gamma=\Sigma_{i=1}^{M}\gamma_i^\dagger\gamma_i$, it is straightforward to see that, in general, either $\exp(i\pi N_c)=\exp(i\pi N_\gamma)$ or $\exp(i\pi N_c)=-\exp(i\pi N_\gamma)$, but to determine which of these holds in a particular instance requires explicit (numerical) calculation. To this end, we consider (restricting ourselves for simplicity to even M) the scalar product of $|\Psi\rangle$ [see Eq. (23)], for which we know that $e^{i\pi N_\gamma}|\Psi\rangle=+|\Psi\rangle$, with a reference state $|\text{ref}\rangle$, chosen in order that $\exp(i\pi N_c)|\text{ref}\rangle=+|\text{ref}\rangle$. The result $\langle\text{ref}|\Psi\rangle\neq 0$ will indicate $e^{i\pi N_c}=e^{i\pi N_\gamma}$, while (barring accidental orthogonality) the result $\langle\text{ref}|\Psi\rangle=0$ implies $\exp(i\pi N_c)=-\exp(i\pi N_\gamma)$. A suitable choice for $|\text{ref}\rangle$ is the state

$$|\text{ref}\rangle=\prod_{i}^{M}(f_i^\dagger+g_i^\dagger)|\text{vac}\rangle, \tag{29}$$

which satisfies $N_C|\text{ref}\rangle=N_D|\text{ref}\rangle=M|\text{ref}\rangle$ and hence also $\exp(i\pi N_c)|\text{ref}\rangle=+|\text{ref}\rangle$. The scalar product is

$$\langle\text{ref}|\Psi\rangle=2^{-M/2}\det(W^T+V)=2^{-M/2}\det(W)\det(1+WV). \tag{30}$$

The only factor on the right side of this expression which may be zero is $\det(1+WV)$. It turns out that $\chi\equiv\det(WV)$,

which takes the values $\chi=\pm1$, is a convenient indicator: barring accidental degeneracies in the spectrum of WV, $\det(1+WV)=0$ if and only if $\chi=-1$.

The proof of this statement is as follows. One has

$$\det(1+WV)=\prod_i (1+\rho_i), \qquad (31)$$

where ρ_i are the eigenvalues of the $O(M)$ matrix WV. These occur as complex conjugate pairs, ρ_i and ρ_i^*, and possibly also as real pairs, 1 and -1, of which there will be at most one in the absence of degeneracy. If there *is* one such real pair, $\chi=-1$ and $\det(1+WV)=0$; if there is none, $\chi=+1$ and $\det(1+WV)\neq0$.

We now apply these results to obtain expressions for the Lyapunov exponents of the Ising model transfer matrix in terms of those of the network model. For simplicity of presentation we make use of a property which appears to hold generally and is certainly true for the model studied in Sec. IV, the $\pm J$ RBIM with $p\leqslant0.5$. In this system, $\chi^+=+1$ always, and half of the Lyapunov exponents λ_i are obtained from Eq. (28) by setting $\epsilon\equiv\epsilon^+$ and taking N_γ even. The remaining exponents result from setting $\epsilon\equiv\epsilon^-$, accompanied by even N_γ if $\chi^-=+1$, and by odd N_γ if $\chi^-=-1$. Since we are concerned in the following only with χ^-, we write it below simply as χ.

Using the expression for the exponents, Eq. (28), we find the following rules for the case $\chi=1$:

$$\lambda_1=\frac{1}{2}\sum_{i=1}^{M} \epsilon_i^+ ,$$

$$\lambda_2=\frac{1}{2}\sum_{i=1}^{M} \epsilon_i^- - \epsilon_1^- ,$$

$$\lambda_3=\frac{1}{2}\sum_{i=1}^{M} \epsilon_i^- - \epsilon_2^- ,$$

$$\lambda_4=\frac{1}{2}\sum_{i=1}^{M} \epsilon_i^+ - \epsilon_1^+ - \epsilon_2^+ . \qquad (32)$$

For the case $\chi=-1$, we have instead

$$\lambda_1=\frac{1}{2}\sum_{i=1}^{M} \epsilon_i^+ ,$$

$$\lambda_2=\frac{1}{2}\sum_{i=1}^{M} \epsilon_i^- ,$$

$$\lambda_3=\frac{1}{2}\sum_{i=1}^{M} \epsilon_i^- - \epsilon_1^- - \epsilon_2^- ,$$

$$\lambda_4=\frac{1}{2}\sum_{i=1}^{M} \epsilon_i^+ - \epsilon_1^+ - \epsilon_2^+ , \qquad (33)$$

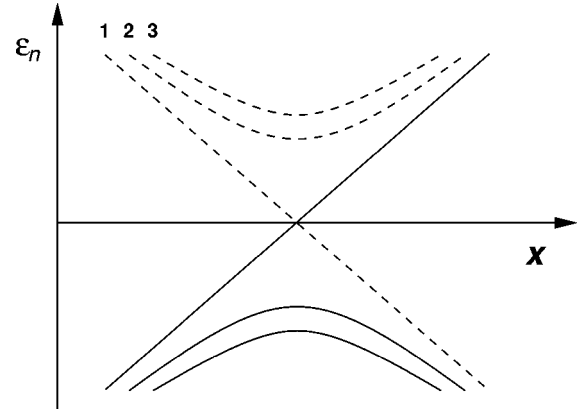where the order of λ_3 and λ_4 has to be decided numerically.

FIG. 4. A sign change of χ as a function of a parameter x is accompanied by the smallest Lyapunov exponent reaching zero. This may be regarded as a form of level crossing, as illustrated.

It is interesting to note a consequence that follows from the importance of χ, and which is probably characteristic of localization problems in class D. It arises if χ can change sign as a continuous parameter, such as temperature in the Ising model, is varied. Since the two subspaces of WV $\in O(M)$ in which $\chi=+1$ and $\chi=-1$, respectively, are disconnected, a change in the sign of χ is accompanied by the vanishing of ϵ_1^-. This process is a form of level crossing, as illustrated in Fig. 4. In the RBIM it occurs for large M at the Curie point, as discussed in Sec. IV.

This distinction between phases with either sign for χ is the analog for the RBIM in cylindrical geometry of a topological classification introduced for two-dimensional systems from class D in Ref. 39 and for one-dimensional, single-channel systems in Ref. 42. In particular, such one-dimensional systems may have two phases: in one phase a long sample supports a zero-energy state at each of its ends, and in the other it does not. Turning to the network model for large L, we note that the combinations $V_L^T W_L^T$ and $W_R V_R$ are the reflection matrices from either end of the system. A closed sample may be constructed in an obvious way, by joining outgoing links to ingoing links in pairs at each end of the system. For a network model, a stationary state has the status of a zero-energy state, and stationary states will exist at the ends of the closed sample if the reflection matrices for the corresponding open system have 1 as an eigenvalue. From the discussion following Eq. (31), one sees that this is the case if $\chi=-1$ but not if $\chi=+1$.

III. CALCULATIONAL METHODS

A. Numerical procedure

Numerical methods suitable for studying random transfer-matrix products in general are well established and described, for example, in Refs. 44–46. It has been recognized recently,[41] however, that these methods may develop an instability to rounding errors and must be modified when applied to systems in symmetry class D. Specifically, the modifications are required if the smallest positive Lyapunov exponent approaches zero on a scale set by the spacing be-

tween other exponents, which happens in the RBIM at the Curie point, as described in Secs. II C and IV. We summarize the established algorithm and review the modification required in this subsection.

First, we define some notation. Consider a network model of width $2M$ links and length L, with a transfer matrix of the form given in Eq. (18). Let $\mathbf{x}^k(n)$, for $k=1,2,\ldots,2M$ and n fixed, be orthonormal column vectors, each of $2M$ components, written in the same basis as this transfer matrix. These vectors are generated by a sequence of operations designed to ensure that $\mathbf{x}^k(L)$ converges for large L to the kth column of the matrix

$$\frac{1}{\sqrt{2}}\begin{pmatrix} W_L & -W_L \\ V_L^T & V_L^T \end{pmatrix} \qquad (34)$$

appearing in the polar decomposition, Eq. (18).

The conventional choice[44-46] for these operations is as follows. Pick $\mathbf{x}^k(0)$ arbitrarily. With $n=0$, let

$$\mathbf{y}^k = T(L-n-s, L-n)\, \mathbf{x}^k(n), \qquad (35)$$

and perform Gram-Schmidt orthonormalization, following

$$\mathbf{z}^k = \mathbf{y}^k - \sum_{i=1}^{k-1} ([\mathbf{x}^i(n+s)]^T \cdot \mathbf{y}^k)\mathbf{x}^i(n+s) \qquad (36)$$

and

$$\mathbf{x}^k(n+s) = \mathbf{z}^k / |\mathbf{z}^k|. \qquad (37)$$

The process is repeated with $n=s, 2s \cdots L-s$. The Lyapunov exponents are then the mean growth rates

$$\epsilon_k = \left\langle \frac{1}{s}\ln|\mathbf{z}^{M+1-k}| \right\rangle \equiv -\left\langle \frac{1}{s}\ln|\mathbf{z}^{M+k}| \right\rangle \qquad (38)$$

for $k=1\cdots M$, where the average is over successive orthonormalization steps. The interval s is taken for computational efficiency to be as large as is possible without rounding errors significantly affecting the orthogonalization.

The rate of approach with increasing L of the vectors $\mathbf{x}^i(L)$ to the columns of Eq. (34) is determined by the spacing between successive Lyapunov exponents. So also are the deviations at large L of these vectors from the columns of Eq. (34). Such deviations are induced by numerical noise and generate errors in the calculated values of Lyapunov exponents. For systems in symmetry class D, the value of the smallest positive Lyapunov exponent, ϵ_1, may approach zero. If it does, the vectors $\mathbf{x}^M(L)$ and $\mathbf{x}^{M+1}(L)$ are unusually susceptible to rounding errors, as is the value of ϵ_1 determined from Eq. (38). We demonstrate in the Appendix that the error decreases with decreasing noise amplitude, σ, only as $|\ln(\sigma)|^{-1}$. Because of this, a modification must be found that stabilizes the algorithm.

Following Ref. 41, we adapt the Gram-Schmidt orthonormalization to enforce the 2×2 block structure evident in Eq. (34). Denoting the jth component of $\mathbf{x}^k(n)$ by $x_j^k(n)$, and similarly for $\mathbf{y}^k$ and $\mathbf{z}^k$, we replace Eq. (36) for $1\leq k\leq M$ by

$$z_j^k = y_j^k - \sum_{i=1}^{k-1} \left(\sum_{l=1}^{M} x_l^i(n+s)y_l^k \right)x_j^i(n+s) \qquad (39)$$

if $1\leq j\leq M$, and by

$$z_j^k = y_j^k - \sum_{i=1}^{k-1} \left(\sum_{l=M+1}^{2M} x_l^i(n+s)y_l^k \right)x_j^i(n+s) \qquad (40)$$

if $M+1\leq j\leq2M$. Similarly, we replace Eq. (37) by

$$x_j^k(n+s) = z_j^k \left/ \left[\sum_{i=1}^{M} |z_i^k|^2 \right]^{1/2} \right., \qquad (41)$$

if $1\leq j\leq M$, and by

$$x_j^k(n+s) = z_j^k \left/ \left[\sum_{i=M+1}^{2M} |z_i^k|^2 \right]^{1/2} \right., \qquad (42)$$

if $M+1\leq j\leq2M$. Lyapunov exponents are determined as before from Eq. (38), and now remain stable to rounding errors even if $\epsilon_1\to0$.

B. Self-averaging quantities

We wish to calculate for the Ising model the free-energy, spin-correlation functions, and correlations of disorder operators. In the presence of bond randomness these all exhibit sample-to-sample fluctuations, but the free-energy density and typical decay lengths appearing in correlations functions are self-averaging. In this subsection we describe how such self-averaging quantities can be obtained from the Lyapunov exponent spectrum of the network model. The calculation of correlation functions themselves is discussed in Sec. III C.

We start from the polar decomposition of the transfer matrix for an (undoubled) Ising model of width M and length L, which [in analogy to Eq. (22)] is

$$\hat{T} = \sum_{l}^{2M} |L_l\rangle e^{\lambda_l L}\langle R_l|. \qquad (43)$$

Defining the reduced free energy per site as

$$F = -\lim_{L\to\infty} \ln(Z)/LM \qquad (44)$$

and using Eqs. (1), (32), and (33), we have by standard arguments

$$F = -\lim_{L\to\infty}\left[\frac{1}{LM}\ln|\mathcal{A}| + \frac{1}{2M}\sum_{i=1}^{M} \epsilon_i^+ \right]. \qquad (45)$$

Turning our attention to typical decay lengths, we note first that, viewing the network model as a localization problem, its smallest positive Lyapunov exponent defines a localization length ξ through $\xi \equiv \epsilon_1^{-1}$. In a localized phase ξ has a finite limit, the bulk localization length, as $M\to\infty$, while at a mobility edge one expects that ξ diverges with M and that a universal scaling amplitude a is defined by the limiting value of $M\epsilon_1$ for $M\to\infty$. An unusual feature of localization problems in symmetry class D is that one may have $a=0$; from

the discussion of Sec. II C and results presented in Sec. IV, this occurs in the RBIM in the sector with odd parity.

For the Ising model, the typical correlation length $\xi_{\sigma\sigma}$ appearing in the spin-spin correlation function may be extracted as follows. This correlator, for two spins with (in the notation of Fig. 1) the same coordinates in the vertical direction and separation n in the horizontal direction, is

$$\langle \sigma_i^x(0)\sigma_i^x(n)\rangle = \frac{\text{Tr}[\sigma_i^x\hat{T}(1,n)\sigma_i^x\hat{T}(n+1,L)]}{\text{Tr}[\hat{T}(1,L)]}. \quad (46)$$

Recalling that σ_i^x has nonzero matrix elements only between states with opposite parity, and taking $L\to\infty$, $\xi_{\sigma\sigma}$ is defined and expressed in terms of the Lyapunov exponents for the spin transfer matrix by

$$\xi_{\sigma\sigma}^{-1} = -\lim_{n\to\infty}\frac{1}{n}\ln(\langle\sigma_i^x(0)\sigma_i^x(n)\rangle) = \lambda_1 - \lambda_2. \quad (47)$$

When writing $\xi_{\sigma\sigma}$ in terms of the network model Lyapunov exponents, it is useful to introduce a length scale ξ_{1D} which characterizes the sensitivity of the network model to changes in boundary conditions, and is defined by

$$\xi_{1D}^{-1} = \frac{1}{2}\sum_i [\epsilon_i^+ - \epsilon_i^-]. \quad (48)$$

We expect insensitivity to boundary conditions except at the critical point, and anticipate that $\xi_{1D}^{-1}\sim\exp(-M/\xi)$ for large M. In regions of the RBIM phase diagram for which $\chi=1$ (corresponding, as we argue, to the paramagnet), we have from Eq. (32)

$$\xi_{\sigma\sigma}^{-1} = \epsilon_1^- + \xi_{1D}^{-1}, \quad (49)$$

so that asymptotically the localization length ξ and spin-correlation length $\xi_{\sigma\sigma}$ are equal. By contrast, in regions of the phase diagram for which $\chi=-1$ (corresponding to the ferromagnet) we have $\xi_{\sigma\sigma}=\xi_{1D}$. This large length scale here characterizes the decay of spin correlations in a quasi-one-dimensional sample within the ordered phase of the two-dimensional system. Such decay is governed by rare domain-wall excitations that cross the width of the sample. Because $\xi_{\sigma\sigma}$ is large when $\chi=-1$, it is useful also to examine the inverse length scale governing corrections to Eq. (47), which is $\lambda_1 - \lambda_3$. For $\chi=-1$

$$\lambda_1 - \lambda_3 = \epsilon_1^- + \epsilon_2^- + \xi_{1D}^{-1}, \quad (50)$$

so that, as $M\to\infty$, $\epsilon_1^- + \epsilon_2^-$ gives the typical decay rate of the connected part of the spin-correlation function in the ordered phase.

In a similar way, one can obtain $\xi_{\mu\mu}$, the typical correlation length for the disorder operators μ_r of Kadanoff and Ceva.[47] These operators are defined at points r which lie at the centers of plaquettes in the Ising model. The two-point correlation function $\langle\mu_0\mu_r\rangle$ is defined by considering a modified system in which exchange interactions crossed by a path on the dual lattice between 0 and r have their sign changed. Then

$$\langle\mu_0\mu_r\rangle = \frac{Z'}{Z} \quad (51)$$

is the ratio of the partition function Z' for the modified system to that of the original system, and

$$\xi_{\mu\mu}^{-1} = -\lim_{r\to\infty}\frac{1}{r}\ln(\langle\mu_0\mu_r\rangle). \quad (52)$$

Because the different boundary conditions imposed on the network model in sectors of even and odd parity constitute an (infinite) line of such modified bonds, $\xi_{\mu\mu}$ may be expressed in terms of ϵ^+ and ϵ^-. Moreover, in the ferromagnetic phase ($\chi=-1$), $\xi_{\mu\mu}$ is the reduced interfacial tension between domains of opposite magnetization. To make this explicit, let F_p and F_a be reduced free energies per site, calculated from the definition Eq. (45) for systems in cylindrical geometry with, respectively, periodic ($\sigma_{M+1}^x\equiv\sigma_1^x$) and antiperiodic ($\sigma_{M+1}^x\equiv-\sigma_1^x$) boundary conditions on spins imposed around the cylinder. Then

$$\xi_{\mu\mu}^{-1} = M(F_p - F_a). \quad (53)$$

In this phase, we find using the ideas of Sec. II C that

$$\xi_{\mu\mu}^{-1} = \epsilon_1^- + \xi_{1D}^{-1}, \quad (54)$$

while in the paramagnetic phase ($\chi=+1$) we obtain $\xi_{\mu\mu}=\xi_{1D}$, so the decay length diverges with M. As one might expect, the behavior of $\xi_{\mu\mu}$ in each phase is similar to that of $\xi_{\sigma\sigma}$ in the dual phase.

C. Correlation functions

Calculation of the full form of correlation functions is more involved than that of the typical decay lengths since, of course, the results cannot be expressed solely in terms of Lyapunov exponents. Nevertheless, it turns out that even powers of correlation functions may be determined straightforwardly.[6] In the most important example of the second power, one requires the product of two equivalent correlation functions, evaluated for each of the two copies of the Ising model that are combined in the network model. In the case of the square of the two-point correlation function of disorder operators, Eq. (51), this means that the same modification of bonds is introduced in both copies of the Ising model, so that $(Z')^2$ is determined from a network model with a specific set of modified nodes. In the case of the square of the spin-spin correlation function, one can take a similar route by expressing this in terms of a disorder correlator in a dual system. Alternatively, one can write the product of two copies of a spin operator in terms of f and g fermions, as we describe below. By either route, one arrives ultimately at the same result: the square of the spin-spin correlation function is given by the ratio of the square of a partition function calculated from a modified network model to the same quantity calculated from an unmodified model. By contrast, odd powers of correlation functions, including the first power, appear to be much harder to evaluate, leaving the sign of the correlation function undetermined: we summarize the difficulties that arise at the end of this subsection.
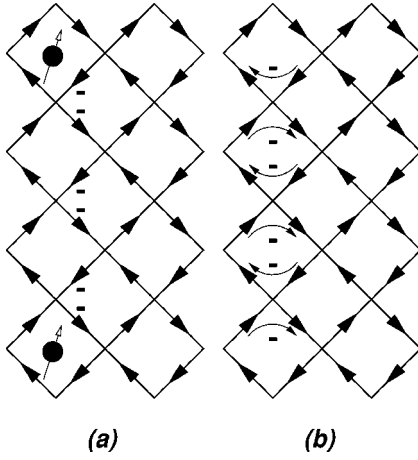
FIG. 5. Schematic representation of the effect of modifying the system by inserting spin operators in one slice: (a) link phases associated with a pair of spin operators; (b) equivalent node phases.

To obtain the squared spin-spin correlation function following Eq. (46), we must evaluate products involving the transfer matrix for the doubled Ising model and also factors of the form $\sigma_{jC}^x \sigma_{jD}^x$. From Eqs. (4) and (7) we have

$$\sigma_{jC}^x \sigma_{jD}^x = i(-1)^j \exp\left(i\pi \sum_{i=1}^{j-1} [f_i^\dagger g_i + g_i^\dagger f_i] + i\pi f_j^\dagger f_j \right). \quad (55)$$

In the spirit of Sec. II B we translate this into first-quantized form. Each operator $\exp(i\pi[f_i^\dagger g_i + g_i^\dagger f_i])$ is represented by a 2×2 matrix, $\exp(i\pi\sigma^x) = -1$. As a result, on one slice of the network model phase factors of -1 are associated with each of the right and left going links having coordinate i in the range $1 \le i \le j-1$. In addition, the operator $\exp(i\pi f_j^\dagger f_j)$ is represented by a similar phase factor associated with the jth right going link. These phase factors are illustrated schematically in Fig. 5(a), using as an example the combination $\sigma_{1C}^x \sigma_{1D}^x \sigma_{4C}^x \sigma_{4D}^x$, which arises in the calculation of $\langle \sigma_i^x(n)\sigma_j^x(m) \rangle^2$ on setting $n = m$, $i = 1$, and $j = 4$. Such link phases can equally be attributed to nodes representing vertical bonds of the Ising model, as indicated in Fig. 5(b). Viewed in this way, the insertion of spin operators into the transfer-matrix product is represented by a change in node parameters $\kappa_{n,i} \to \kappa_{n,i} + i\pi/2$ for $1 \le i \le j-1$. In turn, this is equivalent to a change in sign for the corresponding dual bond strengths, as it should be since the spin-correlation function can be evaluated as a disorder correlator in the dual model.

Implementing this approach in numerical calculations, we determine the singular values of the transfer matrix for modified and unmodified network models of length L, of course using the same realization of disorder for both. From these we calculate the largest singular value of the transfer matrix for the doubled spin system, which we denote by $\exp(2\lambda_1' L)$ in the modified case, and by $\exp(2\lambda_1 L)$ in the unmodified case, following the notation of Sec. II C. For large L

$$\langle \sigma_i^x(n) \sigma_j^x(m) \rangle^2 = \exp(2[\lambda_1' - \lambda_1]L). \quad (56)$$

In practice, the combination $[\lambda_1' - \lambda_1]L$ approaches a finite limiting value rather quickly with increasing L. Conveniently, it is not necessary to evaluate the scalar products of the form $|\langle L_1 | R_1 \rangle|^2$ which appear in the numerator and denominator of Eq. (46), because for large L these are the same in the modified and unmodified systems, and therefore cancel.

As mentioned above, calculation of the unsquared spin-spin correlation function presents greater practical problems. A route is clear in principle: one can use the discussion of Sec. II C to construct the transfer matrix for the undoubled Ising model, via its polar decomposition, in terms of Slater determinants of the γ fermions; and one can also express spin operators in this Ising model in terms of the creation and annihilation operators for these fermions. Difficulties then arise from the fact that the matrices W_L and W_R appearing in Eq. (19) are unrelated in the presence of disorder, as also are V_L and V_R. In consequence, one has to deal with two sets of γ fermions: γ_L and γ_R. Put briefly, we find [as in Eq. (4.7) of Schultz, Mattis, and Lieb[3]] that $\langle \sigma_i^x(n)\sigma_j^x(n) \rangle$ can be written as an expectation value of a product of $2|i-j|$ fermion operators, which can be evaluated using Wick's theorem. However, in the disordered system it is not possible to reduce this expectation value to a single determinant [as in Eq. (4.13) of Ref. 3]. Without such a reduction, the computational effort required to determine $\langle \sigma_i^x(n)\sigma_j^x(n) \rangle$ seems prohibitive for large $|i-j|$.

IV. NUMERICAL RESULTS FOR THE $\pm J$ RBIM

A. Introduction

In this section we present results obtained using the mapping from the Ising model to the network model as a way of studying the $\pm J$ RBIM. Previous work of this type has been described by Cho,[5] but without the advantages of the numerical algorithm or the detailed relation between the network model and statistical mechanical quantities that we have discussed in Sec. III. The $\pm J$ RBIM, defined on a square lattice, has nearest-neighbor exchange couplings J_{ij} drawn independently from the probability distribution

$$P(J_{ij}) = (1-p)\delta(J_{ij} - J) + p\delta(J_{ij} + J), \quad (57)$$

with $0 \le p \le 1$ and J positive; we set $J = 1$ in the following.

The phase diagram of the model, as a function of temperature T and the concentration p of antiferromagnetic bonds, is shown in Fig. 6, with renormalization-group (RG) scaling flow superimposed.[12–29] The pure system ($p = 0$) has a transition between ferromagnetic and paramagnetic phases at a Curie temperature $T_0 = 2[\ln(1+\sqrt{2})]^{-1}$. As antiferromagnetic bonds are introduced the Curie temperature is depressed, and the ferromagnetic phase is destroyed altogether above a threshold concentration p_c. A curve in the $p-T$ plane known as the Nishimori line[14–17] (NL) plays an important role in the discussion of scaling flow. It is defined for the $\pm J$ RBIM by the equation $\exp(2\beta J) = (1-p)/p$. On this line the RBIM has an additional gauge symmetry, because of which the internal energy is analytic and ensemble-averaged spin-spin correlations obey the equalities
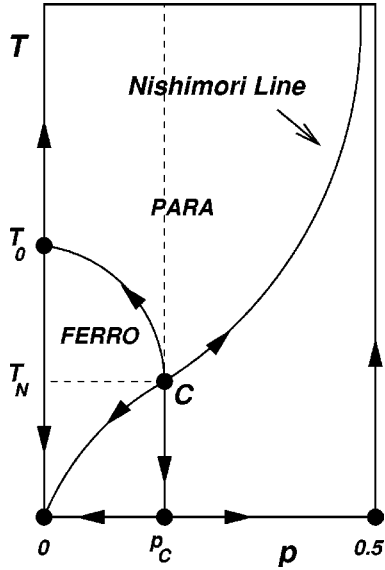
FIG. 6. Phase diagram of the $\pm J$ RBIM with superimposed RG scaling flow.

FIG. 7. The location of the phase boundary determined from numerical calculations. Data obtained on the line $T = 0.68 + 4.67p$ are presented in Fig. 8.

$[\langle \sigma_i^x(n)\sigma_j^x(m)\rangle^{2k-1}] = [\langle \sigma_i^x(n)\sigma_j^x(m)\rangle^{2k}]$ for integer k. The NL cuts the phase boundary separating the ferromagnet from the paramagnet at a point C, the Nishimori point, with coordinates p_c, T_N. This point is particularly interesting as an example of a disorder-dominated multicritial point. One of the two scaling flow axes in its vicinity lies along the NL, while the other coincides with the phase boundary,[16] as indicated in Fig. 6. Scaling flow on the critical manifold for $p < p_c$ runs from the Nishimori point towards the critical fixed point of the pure system, at which disorder is marginally irrelevant. The phase boundary on the other side of the Nishimori point is believed to be vertical[15–17] in the $T-p$ plane, and on it the scaling flow runs from the Nishimori point towards a zero-temperature critical point. Finally, the phase diagram for $p > 1/2$ can be obtained from that shown for $p < 1/2$ by reflection in the line $p = 1/2$, using a gauge transformation which maps p to $1-p$ and the ferromagnetically ordered phase to an antiferromagnet.

Despite the considerable effort which has been invested in studies of the RBIM, some aspects of its behavior are not yet well characterized. In the following, we present a high-accuracy determination of the position of the phase boundary and of critical properties at the Nishimori point.

B. Method

We use the numerical method described in Sec. III A to calculate the Lyapunov exponents of the network model associated with the RBIM, studying two copies of the system for each disorder realization, with boundary conditions appropriate for Fermion numbers of each parity. In the spirit of Sec. III B we use the smallest positive exponent calculated for the network model with periodic boundary conditions to define a characteristic inverse length scale, and analyze the finite-size scaling behavior of $M/\xi = M\epsilon_1^-$ as a function of system width M. In addition, we determine the interfacial
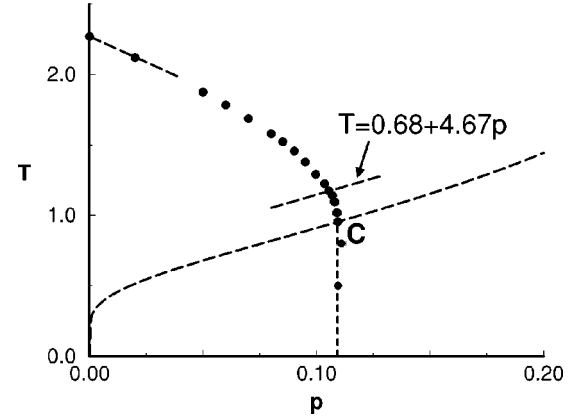
tension $\xi_{\mu,\mu}^{-1}$ and study its size dependence. We also calculate the disorder-averaged square of the spin-spin correlation function, $[\langle \sigma_i^x(n)\sigma_j^x(n)\rangle^2]$, for spins lying in the same slice of the system, using the approach described in Sec. III C.

For most of the results presented, we study system widths in the range from $M = 8$ to $M = 256$ spins, and system lengths of $L = 5 \times 10^5$ spins. Realization-dependent fluctuations in self-averaging quantities decrease as $L^{-1/2}$ and in some cases increase with M. As an example, using $L = 5 \times 10^5$ the value of ϵ_1^- at the Nishimori point is obtained with an accuracy of 1% for $M = 16$ and 2% for $M = 64$. Some calculations require higher precision. In particular, the high-resolution studies of the interfacial tension close to the Nishimori point, presented in Sec. IV D, and of scaling on the phase boundary, presented in Sec. IV E, use systems of length up to $L = 2 \times 10^8$, restricting accessible widths to $M \leqslant 32$.

C. Location of phase boundary

In this subsection we describe the determination of the form of the boundary between the ferromagnetic and paramagnetic phases. We also discuss the nature of finite-size effects in different parts of the phase diagram. For this purpose the quantity χ, introduced in Sec. II C, is very useful and we substantiate our claim that (in the thermodynamic limit) the sign of χ indicates which phase the Ising model is in.

Our results for the position of the phase boundary are shown in Fig. 7 and in Table I. Points on this phase boundary are found from a finite-size scaling analysis of the variation of M/ξ along lines that intersect it; the slopes of these lines in the $p-T$ plane are chosen to avoid crossing the boundary at small angles. Representative data, calculated on the line $T = 0.68 + 4.67p$, are shown in Fig. 8; they have two features that can be used to identify the boundary. First, the curves of M/ξ for two successive values of M have an intersection point, and with increasing M these intersection points approach the boundary from the small-p side. Second, for each M, there is a value of p at which ξ diverges, or equivalently

TABLE I. Location of the phase boundary.

p	T_p	p	T_p
0.005	2.2325 ± 0.0003	0.0903 ± 0.0002	1.458
0.02	2.120 ± 0.001	0.0951 ± 0.0005	1.379
0.05	1.875 ± 0.001	0.1000 ± 0.0005	1.294
0.06	1.783 ± 0.002	0.1035 ± 0.0011	1.224
0.07	1.688 ± 0.002	0.1055 ± 0.0011	1.173
0.08	1.580 ± 0.002	0.1080 ± 0.0021	1.095
0.0852	1.523 ± 0.002	0.1090 ± 0.0021	1.019

$\epsilon_1^- = 0$. With increasing M, these points approach the boundary from the large-p side. We obtain consistent results using the two methods.

A test of these calculations follows from the fact that the tangent to the ferromagnetic-paramagnetic boundary at the pure critical point is known exactly[48] to be $dT_p/dp|_{p=0} = -7.2821\ldots$. From a linear approximation at $p=0.005$ we find $dT_p/dp|_{p=0} = -7.32 \pm 0.06$, in good agreement with this. Our values for T_p are also compatible with those given in Ref. 26.

It is evident from the data shown in Fig. 8, and their equivalent for other values of p and T, that $\epsilon_1^- = 0$ along a line in the phase diagram which approaches the phase boundary for large M, but is displaced from it into the paramagnetic phase for finite M. From the discussion given in Sec. II C, we expect χ to change sign on this same line, being for large M positive in the paramagnetic phase and negative in the ferromagnetic phase. The data shown in Fig. 9 demonstrate that this is so; Fig. 9 also shows that the finite-size shift in the position of the phase boundary is very large in the portion of the phase diagram lying below the NL. It seems possible that these finite-size effects may provide an alternative explanation of data which have been interpreted[23,24] as evidence for a random antiphase state[13] lying in this region of the phase diagram; and it seems likely that they are responsible for nonmonotonic temperature dependence of Lyapunov exponents for the RBIM, reported at $p > p_c$ in Ref. 26.
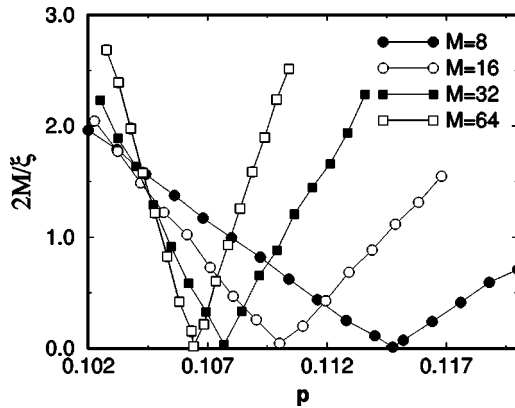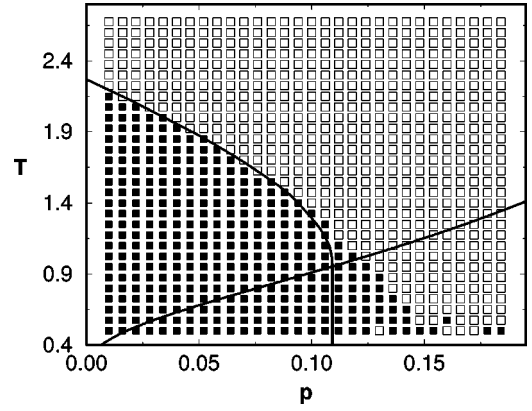

FIG. 9. The sign of χ for a system of width $M = 16$ as a function of position in the $T-p$ plane. Open squares indicate $\chi = +1$ and filled squares $\chi = -1$. The NL and phase boundary are also shown.

D. Nishimori line

In this subsection we examine critical behavior near the multicritical point C as it is approached along the Nishimori line. The facts[15,16] that C is known to lie on the NL, and that the NL coincides with one of the scaling flow axes at C, both greatly help the analysis. We obtain consistent, high-accuracy estimates of the coordinate p_c and the exponent ν using three separate analyses of the finite-size scaling of ξ and also from a study of the interfacial tension.

An overview of the variation of M/ξ along the NL is given in Fig. 10. We apply finite-size scaling ideas to the data in the following different ways. Two of them are similar to the methods used in Sec. IV C to locate the phase boundary: first, curves of M/ξ for two successive values of M cross, and we focus on these crossing points for increasing M; second, for each M there is a point on the NL at which $M/\xi = 0$, and we study the position of these points as a function of M. Third, we can collapse data for different M and from the whole critical region onto a single curve.

Turning to the first of these, we concentrate on the top left of Fig. 10, where data sets intersect roughly at one point. Behavior in this region is shown on a larger scale in Fig. 11. From an extrapolation of the intersection points to large M we find $p_c = 0.1093 \pm 0.0002$. We also obtain a limiting value

FIG. 8. Values of $2M/\xi$ calculated crossing the phase boundary along the line $T = 0.68 + 4.67p$.
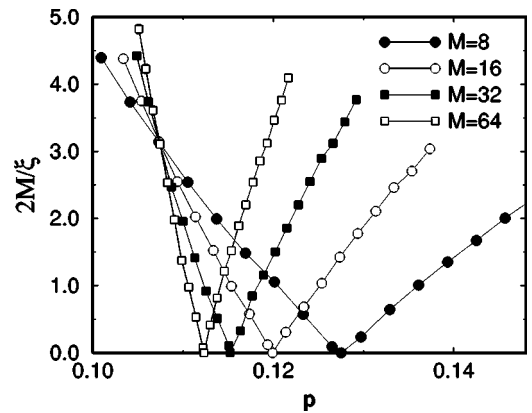

FIG. 10. Variation of $2M/\xi$ along the NL, with position parametrized by p.
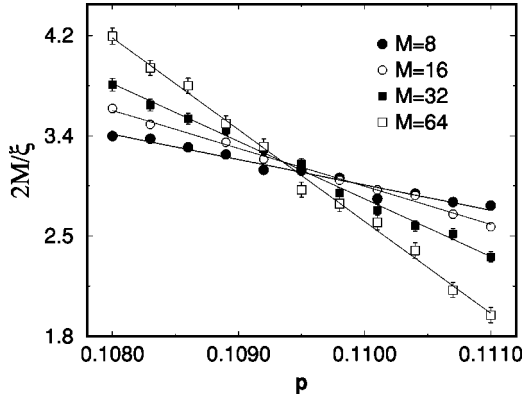
FIG. 11. Variation of $2M/\xi$ along the NL, close to the Nishimori point.

FIG. 13. $\ln(p_M - p_c)$ as a function of $\ln(M)$, for different estimates of p_c. The straightest line is obtained with $p_c = 0.1093$ and has inverse slope -1.49.

at the intersection point of $M/\xi = 1.58 \pm 0.01$ as $M \to \infty$. The value of ν may be found from the scaling with M of the gradients of curves at the intersection points; a similar analysis can also be made for the interfacial tension and we present both together, towards the end of this subsection.

Taking a second approach to the data, the points p_M on the NL at which $M/\xi = 0$ are determined for $8 \leq M \leq 256$ as shown in Fig. 12, where we take advantage of the fact that, for fixed M, the combination $\chi M/\xi$ varies smoothly through zero as a function of position along the NL. One expects the finite-size shift $p_M - p_c$ to vary with M as $(p_M - p_c) \propto M^{-1/\nu}$, and we show the dependence of $p_M - p_c$ on M in Fig. 13, using a double logarithmic scale for various choices of p_c. With the correct choice for p_c, these data should fall onto a straight line of inverse slope $-\nu$. By this method we find $p_c = 0.1093$ and $\nu = 1.49 \pm 0.05$.

A third treatment of the data for M/ξ is provided by attempting to collapse all points from the critical region of Fig. 10 onto a single curve, plotting M/ξ as a function of $(p - p_c)M^{1/\nu}$. In principle, both p_c and ν may be taken as fitting parameters, but we find that p_c is more accurately determined using the methods described earlier. We therefore set $p_c = 0.1093$ and vary only the value of ν. We find the best collapse, shown in Fig. 14, taking $\nu = 1.50$. Visibly worse collapse results from using $\nu = 1.40$, as shown in Fig. 15; by
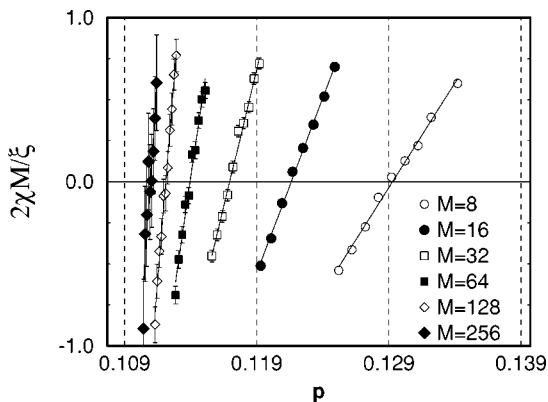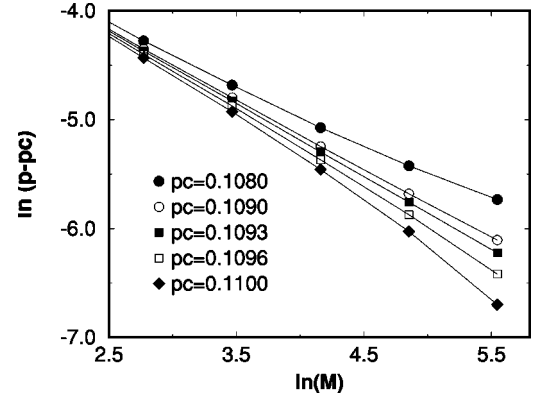
such comparisons we find $\nu = 1.50 \pm 0.10$, confirming the result derived from Fig. 13, but not improving on it in accuracy.

Finally, as a way to check the conclusions we have reached from finite-size scaling of M/ξ, and in order to make a direct comparison with recent work by Honecker, Picco, and Pujol[27] we present a study of the interfacial tension $\xi_{\mu\mu}^{-1}$, defined in Eq. (52). High-precision data, calculated using $L = 2 \times 10^8$ for $8 \leq M \leq 24$ on the NL very close to the Nishimori point, are shown in Fig. 16; statistical errors are smaller than symbol sizes. As with M/ξ, one expects, in the critical region and at sufficiently large M, to collapse data for $M/\xi_{\mu\mu}$ onto a single curve by plotting it as a function of the scaling variable $(p - p_c)M^{1/\nu}$. Such a collapse is illustrated in Fig. 17, using $p_c = 0.1093$ and $\nu = 1.50$. Deviations from collapse are evident at smaller values of M, appearing as vertical offsets of the corresponding lines in Fig. 17. Corrections to scaling of this type are expected, and arise from scaling variables which are irrelevant in the RG sense at the critical point: in general, we have

$$M^2 \Delta f = a + b(p - p_c)M^{1/\nu} + cM^{-x} + \ldots, \qquad (58)$$

where x is the exponent associated with the leading irrelevant scaling variable, a is a universal scaling amplitude, and b and

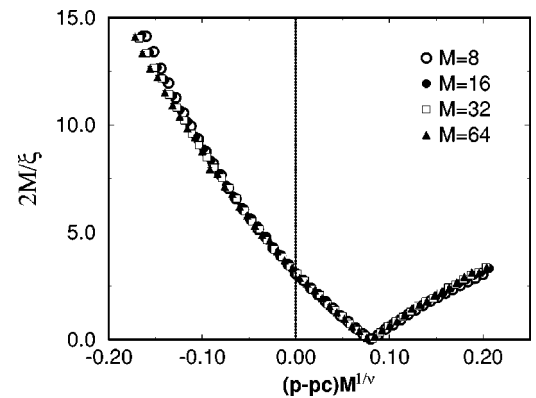FIG. 12. Variation of the combination $2\chi M/\xi$ along the NL.

FIG. 14. Data collapse along the NL, using $\nu = 1.50$ and $p_c = 0.1093$.
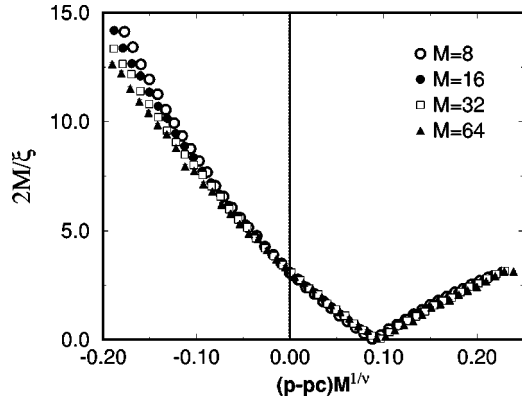
FIG. 15. Data collapse along the NL, using $\nu=1.40$ and $p=0.1093$.

FIG. 17. Scaling of $M/\xi_{\mu\mu}$ as a function of $(p-p_c)M^{1/\nu}$, using $\nu=1.50$ and $p_c=0.1093$.

c are constants. Such corrections occur at the pure Ising transition,[34] and have also been studied in the U(1) network model.[49] In view of the way that they enter Eq. (58), it is appropriate to concentrate on the M dependence of the gradients of lines in Fig. 16 when determining ν. These gradients are shown as a function M using a double logarithmic scale in Fig. 18, from which we derive our most precise estimate of ν, $\nu=1.50\pm0.03$.

The scaling of M/ξ close to the critical point can be analyzed in just the same way, yielding the same result for ν. This scaling collapse is depicted in Fig. 19.

We conclude our analysis of critical behavior on the Nishimori line with the results $p_c=0.1093\pm0.0002$ and $\nu=1.50\pm0.03$. Our value for p_c is consistent with the result $p_c=0.1094\pm0.0002$, obtained by Honecker, Picco, and Pujol,[27] who carried out a detailed study of the interfacial tension and correlation functions, using the Ising model transfer matrix in a spin basis, which restricted system widths to $M\leqslant12$. Our value for p_c is also in agreement with some earlier, less precise values, including $p_c=0.111\pm0.002$, in Ref. 23 and $p_c=0.1095\pm0.0005$ in Ref. 26, both found using a transfer-matrix approach with up to 14 spins. It is also marginally in agreement with $p_c=0.104$ from Ref. 29 obtained as the critical disorder strength around $T=0$. It is in marginal disagreement with the result from series expansions,[18] $p_c=0.114\pm0.003$. More strikingly, however,
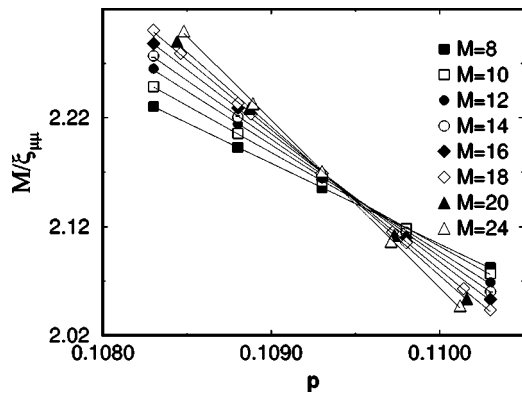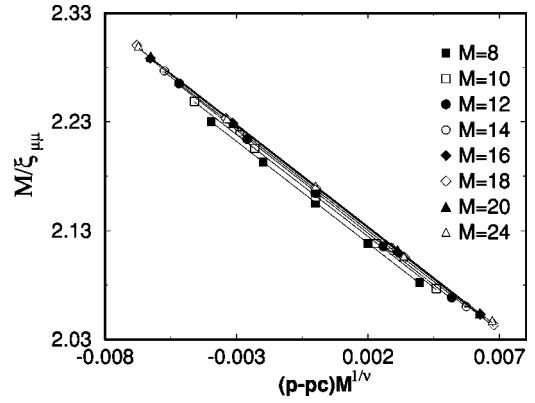
our value for ν is in disagreement with previous estimates, which lie close[18] to the percolation value, $\nu=4/3$, including most recently $\nu=1.33\pm0.03$ in Ref. 27. We believe that the larger system sizes accessible in our work, and the allowance we have made for irrelevant scaling variables at the critical point, together account for the discrepancy, and that the data shown in Figs. 15 and 18 exclude this smaller value of ν.

E. Scaling along the phase boundary

The phase boundary separating the ferromagnet from the paramagnet coincides[16] with the second relevant scaling axis at the Nishimori point, in addition to that defined by the NL. On the boundary, we expect scaling flow from C towards the pure critical point for $p<p_c$, and from C towards the zero-temperature critical point for $T<T_N$. We analyze such flow in this subsection.

Qualitative evidence in support of these established ideas is presented in Fig. 20, which shows the variation of M/ξ with position, parametrized by T, on the phase boundary, and with M. For $p<p_c$, the coordinates of points on the phase boundary are taken from Table I, while for $T<T_N$ we assume the phase boundary to be vertical in the $p-T$ plane and set $p=p_c$, using our estimate for the value of p_c. At temperatures $T>T_N\simeq0.9533$, M/ξ decreases with increasing M, ap-

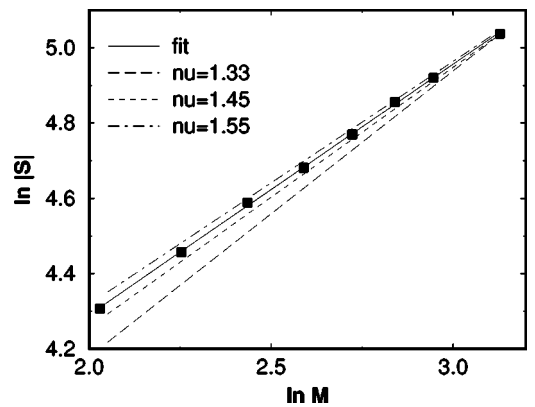FIG. 16. Variation of $M/\xi_{\mu\mu}$ on the NL close to the Nishimori point.

FIG. 18. Scaling of the gradient S of lines in Fig. 16 as a function of M. The best-fit inverse slope is $\nu=1.50$ (solid line). Lines corresponding to $\nu=1.33$, 1.45, and 1.55 are also shown.
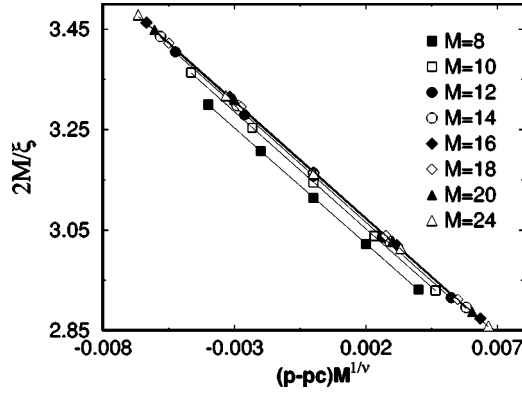
FIG. 19. Scaling of M/ξ on the NL close the the Nishimori point, using $\nu = 1.50$ and $p_c = 0.1093$.

proaching zero which is the value taken by this scaling amplitude in the pure Ising model at $T = T_0 \simeq 2.269$; fluctuations visible in Fig. 20 for data at temperatures $T \gtrsim 1.5$ arise from errors in determining the position of the phase boundary. At the Nishimori point itself, curves of M/ξ for different M cross, with a limiting value for $M \rightarrow \infty$, as already determined in our study of behavior on the NL. For $T < T_N$, values of M/ξ increase both with decreasing T and with increasing M, as expected if flow is towards lower temperatures.

Scaling flow along the phase boundary close to the Nishimori point is characterized by a critical exponent ν_T, which in principle can be determined using an approach similar to that taken for ν. In practice, there are extra difficulties. First, in contrast to the NL, the form of the phase boundary is not known exactly; we choose the simpler regime, $T < T_N$, and set p to our estimate for p_c, as above. Second, it happens that $\nu_T > \nu$, so that flow away from the multicritical point is faster in the direction of the NL than along the phase boundary. Because of this, the range for T over which useful data can be collected is limited on both sides. The distance, $T_N - T$, from the Nishimori point should not be too large, or data will lie outside the critical region. It should not be too small either, because close to C errors in our value for p_c will be dominant. Having limited the range for $T - T_N$ in this way, the variation in M/ξ is also restricted. It is therefore
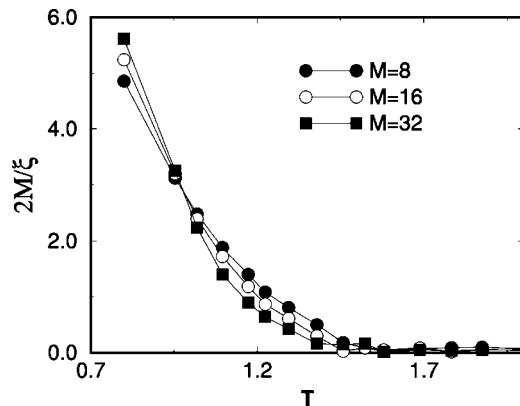
particularly important that statistical errors are small, and so we study samples of length $L = 2 \times 10^8$ with $8 \leqslant M \leqslant 32$. The scaled data are presented in Fig. 21: as with the analysis presented in Figs. 17 and 19, and as expected from Eq. (58), the value of ν_T is determined mainly from the gradients of curves for each M. We conclude that $\nu_T = 4.0 \pm 0.5$. While this confidence margin is wide, it is encouraging that on extrapolating the data in Fig. 21 to $T = T_N$ we obtain at the Nishimori point $M/\xi = 1.58 \pm 0.01$ for $M \rightarrow \infty$, in perfect agreement with the value found independently from data collapse on the NL. The result $\nu_T = 4.0$ is also in agreement with the estimate for the ratio α/ν_T obtained in Ref. 26 from finite size scaling of the specific heat. The exponents α and ν_T are related by the hyperscaling relation $d\nu_T = 2 - \alpha$ and the value $\alpha/\nu_T = -1.5$ in Ref. 26 gives exactly $\nu_T = 4.0$.

F. Behavior at strong disorder

In three or more dimensions, the random-bond Ising model has a spin-glass phase at low temperature and strong disorder.[50] It is known that spin-glass order does not occur in the two-dimensional RBIM, except at zero temperature,[50] but it is of interest to examine behavior at strong disorder using the methods we have developed.

Finite-size effects in the RBIM are large at strong disorder and low temperature, as remarked in connection with Fig. 9, and as is clear from Fig. 22, which shows the variation of
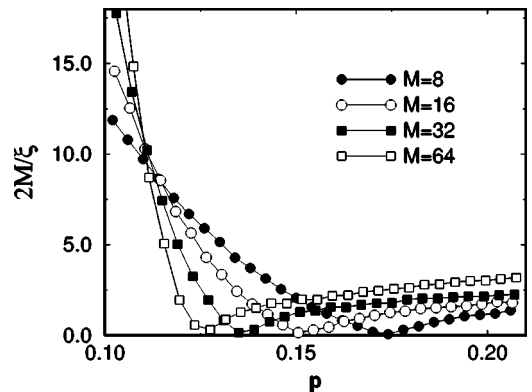

FIG. 21. Scaling of M/ξ on the phase boundary below the Nishimori point, using $\nu_T = 4.0$ and $T_N = 0.9533$.

FIG. 20. Variation of M/ξ with position, parametrized by T, on the phase boundary.

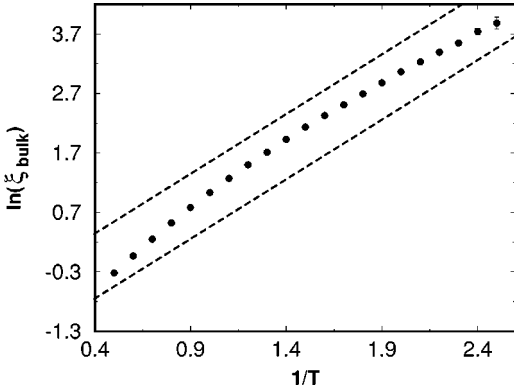FIG. 22. Variation of M/ξ with p, crossing the phase boundary at $T = 0.5$.

FIG. 23. Variation of ξ_{bulk} with T on the line $p=0.5$: $\ln(\xi_{bulk})$ as a function of $1/T$. Dashed lines represent $\xi_{bulk} \propto \exp(2/T)$.

M/ξ with p and M at a fixed temperature, $T=0.5$, below the Nishimori point. Despite these finite-size effects, it is straightforward to identify the position of the phase boundary from Fig. 22. Moreover, the size dependence of M/ξ in the paramagnetic phase at $T=0.5$ and higher temperatures is consistent with a finite limiting value for ξ as $M \to \infty$, as required from the fact that the RBIM does not have a metallic phase.[6]

For a quantitative analysis of behavior in this region, we focus on the line $p=0.5$ which, by symmetry arguments, is an exact scaling axis. Scaling flow is from the zero-temperature fixed point at $p=0.5$ towards infinite temperature, and one can collapse data on this line to extract the limiting behavior of ξ for $M \to \infty$. This extrapolated localization length ξ_{bulk} is expected to be finite for $T>0$. Its temperature dependence for $T \geqslant 0.4$ (obtained using $8 \leqslant M \leqslant 64$ and $L=10^6$) is shown in Fig. 23, where we compare our results with the behavior $\xi_{bulk} \propto \exp(2/T)$, suggested[32,51] for the $\pm J$ RBIM. In Fig. 24 we compare our same results with the power-law divergence, $\xi_{bulk} \propto T^{-\nu}$, expected in a RBIM with a distribution of bond strengths continuous at $J=0$, for which exponent values in the range $\nu=3.4-\nu=4.2$ have been reported previously.[22,52,53] Our data in the temperature range accessible do not provide firm grounds to prefer one form for the temperature dependence over the other.
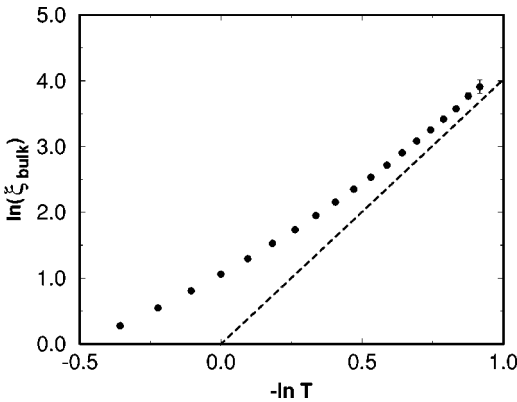

FIG. 24. Variation of ξ_{bulk} with T on the line $p=0.5$: $\ln(\xi_{bulk})$ as a function of $\ln(T)$. The dashed line represents $\xi_{bulk} \propto T^{-\nu}$ with $\nu=4$.
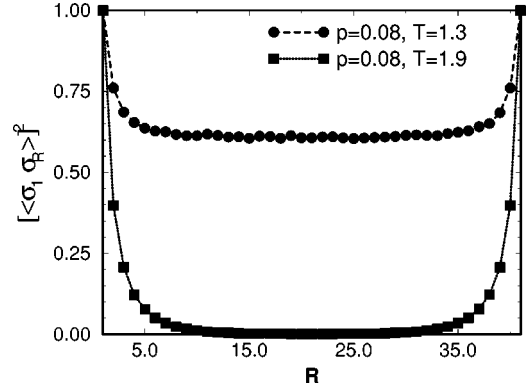

FIG. 25. Variation of the disorder-averaged square spin-spin correlation function with distance around a system of circumference $M=40$, in the paramagnetic phase ($T=1.9$) and the ferromagnetic phase ($T=1.3$).

G. Spin-spin correlations

As a demonstration of the effectiveness of the method set out in Sec. III C for obtaining even powers of spin-spin correlation functions, we have calculated $[\langle \sigma_i^x(n)\sigma_j^x(n)\rangle^2]$ at all separations $|i-j|$ of spins across the width of a long system with $M=40$. Data at $p=0.08$, obtained by averaging over 10^4 disorder realizations, are shown in Fig. 25, for a high temperature, $T=1.9$, lying in the paramagnetic phase, and for a lower temperature, $T=1.3$, lying in the ferromagnetic phase. It is clear for this second case that the value of the square of the magnetization can be obtained from the correlation function at separations close to $M/2$.

We have also used this approach to calculate $[\langle \sigma_i^x(n)\sigma_j^x(n)\rangle^2]$ and $[\langle \sigma_i^x(n)\sigma_j^x(n)\rangle^4]$ on the NL at our estimated position for the Nishimori point. At this point, one expects decay of the disorder-average of the kth power of the spin-spin correlation function to be characterized by an exponent η_k. Following the analysis described in Ref. 27, and taking $M=20$, L large, and 10^4 realizations, we obtain $\eta_2 = 0.183 \pm 0.003$ and $\eta_4 = 0.253 \pm 0.003$, in agreement with earlier results.[27]

V. SUMMARY

To summarize, we have described in detail a mapping between the two-dimensional random-bond Ising model and a network model with the symmetries of class D localization problems. Building on Refs. 4–7 we have shown in particular how separate boundary conditions arise in the network model for sectors of the Ising model transfer matrix with even and odd parity under spin reversal, and how statistical-mechanical quantities, including the free energy per site and correlation functions, may be obtained from calculations using the network model. Among other things, this makes clear the sense in which the Ising model correlation length may be equated with the network model localization length. From a computational viewpoint, calculations based on the network model are much more efficient than their equivalent using an Ising model transfer matrix in a spin basis. This is illustrated by the fact that such calculations have in the past mainly been restricted to systems of width $M \leqslant 14$ spins, while we present results in this paper for $M \leqslant 256$ spins. Applying

these ideas to study the Nishimori point for the $\pm J$ RBIM, we obtain a value for the exponent ν which is significantly different from previous estimates based on much smaller systems sizes; our value excludes the possibility of a simple connection between behavior at this critical point and classical percolation, conjectured previously.[18] Beyond computational advantages, the equivalence between the RBIM and the network model has theoretical interest. It links the transition between paramagnet and ferromagnet to a version of the quantum Hall plateau transition, as our results illustrate. Moreover, even in quasi-one-dimensional systems for which there is no sharp Curie transition, a topological distinction emerges within the network model between two separate localized phases.

APPENDIX: EFFECT OF ROUNDING ERRORS ON LYAPUNOV EXPONENTS

The numerical results presented in this paper were obtained using a modified version of the standard algorithm for studying random matrix products, as we describe Sec. III A. The need for such a modification stems from the instability of the standard algorithm to rounding errors if the value of the smallest positive Lyapunov exponent, ϵ_1, approaches zero. The instability is extreme and it is of interest to understand how it arises. In this Appendix we illustrate its origin by examining a simple model problem.

It is sufficient to consider only products of 2×2 matrices, because the instability involves only the space spanned by the vectors associated with the pair of Lyapunov exponents smallest in magnitude, denoted by $\mathbf{x}^M(L)$ and $\mathbf{x}^{M+1}(L)$ in Sec. III A. We therefore consider a product of random matrices, each of the form

$$T_n = \begin{pmatrix} \cosh \theta_n & \sinh \theta_n \\ \sinh \theta_n & \cosh \theta_n \end{pmatrix} \tag{A1}$$

and drawn independently from a distribution which has $\langle \theta_n \rangle = 0$ in order that the Lyapunov exponents of the matrix product are zero. To model the operation of the standard algorithm, we consider evolution of a two-component vector $\mathbf{v}_n$ under an analog of Eqs. (35)–(37):

$$\mathbf{v}_{n+1} = \frac{T_n \mathbf{v}_n}{|T_n \mathbf{v}_n|}. \tag{A2}$$

In the absence of rounding errors, $\mathbf{v}_n$ converges with increasing n to one of the eigenvectors of T_n, and so it is natural to expand $\mathbf{v}_n$ in this basis, writing

$$\mathbf{v}_n = \frac{1}{\sqrt{2}} \begin{pmatrix} 1 \\ 1 \end{pmatrix} \cos \phi_n + \frac{1}{\sqrt{2}} \begin{pmatrix} 1 \\ -1 \end{pmatrix} \sin \phi_n. \tag{A3}$$

In this notation, Eq. (A2) may be written $\tan \phi_{n+1} = \exp(-2\theta_n)\tan \phi_n$, and has fixed points $\phi_n = m\pi/2$ with m integer. We concentrate on the vicinity of one of these, considering the range $0 \leq \phi_n \ll 1$. Then $\phi_{n+1} \approx \exp(-2\theta_n)\phi_n$. We take the effect of rounding errors into account by substituting for this the evolution equation

$$\phi_{n+1} = \exp(-2\theta_n)\phi_n + \eta_n, \tag{A4}$$

where η_n is random with $\langle \eta_n \rangle = 0$ and $\langle \eta_n \eta_m \rangle = \delta_{mn}\sigma^2$.

A simple treatment of the stochastic process defined in this way is sufficient for our purposes. To find approximately the limiting distribution $P(\phi_n)$ at large n, we divide the range under consideration for ϕ_n into the regimes $0 \leq \phi_n < \sigma$ and $\sigma < \phi_n$. In the former the noise dominates, generating an approximately uniform distribution for ϕ_n. We take

$$P(\phi_n) = C_1, \tag{A5}$$

where C_1 is a constant. In the latter regime we neglect the noise and use in place of ϕ_n the variable $y_n = \ln(\phi_n)$, taking its evolution to be

$$y_{n+1} = y_n - 2\theta_n. \tag{A6}$$

Since we have chosen $\langle \theta_n \rangle = 0$, this generates a uniform distribution for y_n in the range $\sigma \leq y_n \leq Y$, where the upper limit $Y \sim \ln(\pi/4)$ represents the point at which the linearization of $\tan(\phi_n)$ fails, and also the boundary separating the vicinities of the fixed points of Eq. (A2) at $\phi_n = 0$ and at $\phi_n = \pi/2$. On transforming back to ϕ_n we obtain within our approximations

$$P(\phi) = \begin{cases} C_1 & \text{for } 0 < \phi < \sigma \\ C_2/\phi & \text{for } \sigma < \phi < \pi/4, \end{cases} \tag{A7}$$

where $C_2 = C_1 \sigma$ for continuity. C_1 is determined by the normalization condition

$$\int_0^{\pi/4} P(\phi_n)d\phi_n = \frac{1}{2} \tag{A8}$$

since we may take the full range for ϕ_n to be $0 < \phi_n < \pi/2$. We find for $\sigma \ll 1$

$$C_1 \simeq [2\sigma \ln(\pi/4\sigma)]^{-1}. \tag{A9}$$

Now consider the effect that noise-induced departures of ϕ_n from the fixed point at $\phi_n = 0$ have on the estimate of the Lyapunov exponent, ϵ. Using $\epsilon = \langle \ln|T_n\mathbf{v}_n| \rangle$, we have

$$\epsilon = \frac{1}{2}\langle \ln[\exp(2\theta_n)\cos^2\phi_n + \exp(-2\theta_n)\sin^2\phi_n] \rangle. \tag{A10}$$

Taking for simplicity θ_n and ϕ_n small, we find

$$\epsilon \simeq 4\langle \phi_n^2 \rangle \langle \theta_n^2 \rangle. \tag{A11}$$

In the absence of noise, $\phi_n = 0$ and hence $\epsilon = 0$. With noise present we must evaluate

$$\langle \phi_n^2 \rangle = \int_0^{\pi/4} P(\phi_n) \phi_n^2 d\phi_n. \tag{A12}$$

Using our approximate form for $P(\phi_n)$ we find, for $\sigma \ll 1$, $\langle \phi_n^2 \rangle \propto |\ln(\sigma)|^{-1}$ and hence

$$\epsilon \propto |\ln(\sigma)|^{-1}. \tag{A13}$$

Thus small rounding errors may be responsible for a large error in the value obtained for the Lyapunov exponent. In the language of this Appendix, the modified algorithm described in Sec. III A uses the known symmetry of the transfer matrix to fix $\phi_n = 0$.

[1] R.J. Baxter, *Exactly Solved Models in Statistical Mechanics* (Academic Press, New York, 1982).

[2] B.M. McCoy and T.T. Wu, *The Two-Dimensional Ising Model* (Harvard University Press, Cambridge, MA, 1973).

[3] T.D. Schultz, D. Mattis, and E.H. Lieb, Rev. Mod. Phys. **36**, 856 (1964).

[4] S. Cho and M.P.A. Fisher, Phys. Rev. B **55**, 1025 (1997).

[5] S. Cho, Ph.D. thesis, University of California, Santa Barbara, 1997.

[6] N. Read and A.W.W. Ludwig, Phys. Rev. B **63**, 024404 (2001).

[7] I.A. Gruzberg, N. Read, and A.W.W. Ludwig, Phys. Rev. B **63**, 104422 (2001).

[8] Vik.S. Dotsenko and Vl.S. Dotsenko, Adv. Phys. **32**, 129 (1983).

[9] B.N. Shalaev, Fiz. Tverd. Tela (Leningrad) **26**, 3002 (1984) [Sov. Phys. Solid State **26**, 1811 (1984)]; Phys. Rep. **237**, 129 (1994).

[10] R. Shankar, Phys. Rev. Lett. **58**, 2466 (1987).

[11] A.W.W. Ludwig, Phys. Rev. Lett. **61**, 2388 (1988).

[12] A.P. Young and B.W. Southern, J. Phys. C **10**, 2179 (1977).

[13] R. Maynard and R. Rammal, J. Phys. (France) Lett. **43**, L347 (1982).

[14] H. Nishimori, Prog. Theor. Phys. **66**, 1169 (1981).

[15] H. Nishimori, J. Phys. Soc. Jpn. **55**, 3305 (1986).

[16] P. Le Doussal and A.B. Harris Phys. Rev. Lett. **61**, 625 (1988).

[17] H. Kitatani, J. Phys. Soc. Jpn. **61**, 4049 (1992).

[18] R.R.P. Singh and J. Adler, Phys. Rev. B **54**, 364 (1996).

[19] Y. Ozeki and H. Nishimori, J. Phys. Soc. Jpn. **56**, 1568 (1987).

[20] J. Houdayer, Eur. Phys. J. B **22**, 479 (2001).

[21] I. Morgenstern and K. Binder, Phys. Rev. B **22**, 288 (1980).

[22] W.L. McMillan, Phys. Rev. B **29**, 4026 (1984).

[23] Y. Ozeki and H. Nishimori, J. Phys. Soc. Jpn. **56**, 3265 (1987).

[24] Y. Ueno and Y. Ozeki, J. Stat. Phys. **64**, 227 (1991).

[25] H. Kitatani and T. Oguchi, J. Phys. Soc. Jpn. **61**, 1598 (1992).

[26] F.D.A.A. Reis, S.L.A. de Queiroz, and R.R. dos Santos, Phys. Rev. B **60**, 6740 (1999).

[27] A. Honecker, M. Picco, and P. Pujol, Phys. Rev. Lett. **87**, 047201 (2001).

[28] Y. Ozeki, J. Phys. Soc. Jpn. **59**, 3531 (1990).

[29] N. Kawashima and H. Rieger, Europhys. Lett. **39**, 85 (1997).

[30] J.A. Blackman, Phys. Rev. B **26**, 4987 (1982).

[31] J.A. Blackman and J. Poulter, Phys. Rev. B **44**, 4374 (1991); J.A. Blackman, J.R. Goncalves, and J. Poulter, Phys. Rev. E **58**, 1502 (1998).

[32] L. Saul and M. Kardar, Phys. Rev. E **48**, R3221 (1993); Nucl. Phys. B **432**, 641 (1994).

[33] M. Inoue, J. Phys. Soc. Jpn. **64**, 3699 (1995).

[34] E.S. Sorensen, cond-mat/0006233 (unpublished).

[35] J.T. Chalker and P.D. Coddington, J. Phys. C **21**, 2665 (1988).

[36] M.R. Zirnbauer, J. Math. Phys. **37**, 4986 (1996); A. Altland and M.R. Zirnbauer, Phys. Rev. B **55**, 1142 (1997).

[37] R. Bundschuh, C. Cassanello, D. Serban, and M.R. Zirnbauer, Phys. Rev. B **59**, 4382 (1999).

[38] T. Senthil and M.P.A. Fisher, Phys. Rev. B **61**, 9690 (2000).

[39] N. Read and D. Green, Phys. Rev. B **61**, 10 267 (2000).

[40] M. Bocquet, D. Serban, and M.R. Zirnbauer, Nucl. Phys. B **578**, 628 (2000).

[41] J.T. Chalker, N. Read, V. Kagalovsky, B. Horovitz, Y. Avishai, and A.W.W. Ludwig, cond-mat/0009463 (unpublished).

[42] O. Motrunich, K. Damle, and D.A. Huse, Phys. Rev. B **63**, 224204 (2001).

[43] J.B. Zuber and C. Itzykson, Phys. Rev. D **15**, 2875 (1977).

[44] G. Benettin, L. Galgani, A. Giorgilli and J.-M. Strelcyn, Meccanica **15**, 9 (1980).

[45] J.L. Pichard and G. Sarma, J. Phys. C **17**, 4111 (1981).

[46] A. MacKinnon and B. Kramer, Phys. Rev. Lett. **47**, 1546 (1981); Z. Phys. B: Condens. Matter **53**, 1 (1983).

[47] L.P. Kadanoff and H. Ceva, Phys. Rev. B **3**, 3918 (1971).

[48] E. Domany, J. Phys. C **12**, L119 (1979).

[49] J.T. Chalker and J. Eastmond (unpublished); J. Eastmond, D. Phil. thesis, Oxford University, 1992; B. Huckestein, Phys. Rev. Lett. **72**, 713 (1994).

[50] A.P. Young and K. Binder, Rev. Mod. Phys. **58**, 801 (1986).

[51] A.J. Bray (private communication).

[52] A.J. Bray and M.A. Moore, J. Phys. C **17**, L463 (1984).

[53] D.A. Huse and I. Morgenstern, Phys. Rev. B **32**, 3032 (1985).